Cooperative action of miR-124 and ISX9 in instructing direct reprogramming of mouse astrocytes to induced-neurons in vitro and in vivo

Elsa Papadimitriou[1], Paraskevi N. Koutsoudaki[1,&], Timokratis Karamitros[2,*], Dimitra Karagkouni[3,*], Dafni Chroni-Tzartou[4], Maria Margariti[1], Christos Gkemisis[1], Evangelia Xingi[5], Irini Thanou[1], Socrates J. Tzartos[4], Artemis G. Hatzigeorgiou[3], Dimitra Thomaidou[1,5,#]

Affiliations

[1]Neural Stem Cells and Neuro-imaging Group, Department of Neurobiology, Hellenic Pasteur Institute

[2]Bioinformatics and Applied Genomics Unit, Department of Microbiology, Hellenic Pasteur Institute

[3]DIANA-Lab, Hellenic Pasteur Institute & Dept. of Computer Science and Biomedical Informatics, Univ. of Thessaly

[4]Laboratory of Molecular Neurobiology and Immunology, Department of Neurobiology, Hellenic Pasteur Institute

[5]Light Microscopy Unit, Hellenic Pasteur Institute

*equally contributing authors

[&]Present address: Molecular Carcinogenesis Group, Department of Histology and Embryology, Medical School, National and Kapodistrian University of Athens, Athens, Greece

[#]Corresponding author

Email: thomaidou@pasteur.gr

Abstract

miR-124 plays a major regulatory role in neurogenesis and neuronal differentiation during brain development through control of its multiple non-neuronal targets and has therefore been employed in direct reprogramming protocols supplementary to neurogenic TFs, and other miRNAs to enhance neurogenic conversion. However, its capacity to instruct neurogenic conversion of astrocytes and its independent mechanism of direct reprogramming action have been poorly investigated. Aim of the study was to investigate whether miR-124 is a master-regulatory reprogramming agent, potent to drive direct reprogramming of astrocytes to induced-neurons (iNs) on its own and to elucidate its mechanism of reprogramming action. To this end we overexpressed miR-124 either alone or in combination with the small neurogenic compound ISX9 both in vitro and in in vivo in a mouse mechanical cortical trauma model and analyzed their mechanism of reprogramming action. Our data indicate that miR-124 and ISX9 exhibit both unique and convergent molecular contributions in the reprogramming process to iNs. miR-124 is a potent driver of the astrocytic reprogramming switch of astrocytes towards an immature neuronal fate by repressing genes regulating astrocytic function, among which we identified the RNA-binding protein Zfp36l1 as a novel miR-124 direct target. We also provide evidence that ISX9 greatly improves both miR-124-induced reprogramming efficiency and functional maturation of iNs. Importantly, miR-124 either alone or along with ISX9 is potent to guide direct neuronal reprogramming of reactive astrocytes to iNs of cortical identity in vivo, a novel finding confirming the robust direct reprogramming action of the two molecules in activated astrocytes in vivo.

Introduction

Direct reprogramming has emerged as a promising approach for manipulating cell fate towards induced-neurons (iNs) maintaining their intrinsic epigenetic signature (Huh et al., 2016), which is particularly important for the study of neurodegenerative disorders primarily affecting the aging population. Astrocytic reprogramming to iNs in particular takes advantage of the intrinsic neural stem cell potential of reactive astrocytes (Magnusson et al., 2014), while it offers the possibility of reprogramming resident brain cells. To this end astrocytic cell fate conversion to iNs has been well-established in vitro (Aravantinou-Fatorou et al., 2015; Berninger et al., 2007; Heinrich et al., 2010) and to some extent in vivo (Guo et al., 2014; Mattugini et al., 2019; Torper et al., 2013) using combinations of transcription factors (TFs) or chemical cocktails (Gao et al., 2017; Xiang Li et al., 2015; Lei Zhang et al., 2015). Challenging the expression of lineage-specific TFs during reprogramming, has been shown to be accompanied by changes in the expression of regulatory RNAs, suggesting that the latter act as key regulators of cell fate conversion (Xuekun Li & Jin, 2010). To this end, miRNAs have been introduced, supplementary or alternatively to TFs, to instruct direct neuronal reprogramming (Yoo et al., 2011). Indeed miRNAs are efficient cell fate conversion factors largely due to the global effects they exert on gene transcription regulatory networks through simultaneous post-transcriptional modulation of high numbers of neurogenesis-promoting factors (Xuekun Li & Jin, 2010).

Among neurogenic miRNAs, miR-124 has been shown to contribute to efficient neurogenic conversion of fibroblasts when coupled with certain TFs or other miRNAs, in particular miR-9/9*(Abernathy et al., 2017; Ambasudhan et al., 2011; Victor et al., 2014; Wohl & Reh, 2016). miR-124 is the most abundant miRNA in the CNS, playing important role both in embryonic neurogenesis (Maiorano & Mallamaci, 2009) and adult neurogenesis (Åkerblom et al., 2012; Cheng et al., 2009), while its expression persists in mature neurons (Deo et al., 2006). Its mechanism of action has been studied over the years, where it has been shown to act globally to increase the expression levels of neuronal genes, by repressing components of major neuronal gene repressor complexes, such as the anti-neural transcriptional repressor REST complex, targeting Scp1 and Rcor1 (Baudet et al., 2012; Visvanathan et al., 2007; Volvert et al., 2014) and the Polycomb Repressive Complex 2 (PRC2), repressing the histone 3 lysine 27 methyltransferase Ezh2 (Lee et al., 2018; Neo et al., 2014), while it also participates at the post-transcriptional regulation of neuronal transcripts by targeting the neuron-specific splicing global repressor Ptbp1 (Makeyev et al., 2007). Besides its roles in

transcriptional and post-transcriptional regulation, miR-124 neurogenic action also relates to chromatin dynamics, as it has emerged as one of the key mediators of a chromatin permissive environment for neuronal reprogramming through its involvement in the formation of the neuron specific chromatin remodeling complex nBAF, by targeting BAF53a subunit mediating its exchange with its homologous, neuronal specific BAF53b (Tang et al., 2013a; Yoo et al., 2009a).

However, although miR-124 has been lately considered as a key reprogramming agent in fibroblast neurogenic conversion protocols, neither its potential to induce fate conversion of astrocytes to iNs in vitro or in vivo, nor its mechanism of action in instructing direct reprogramming on its own have been investigated. In this study we show that miR-124 is potent to reprogram cortical astrocytes to immature neurons, however it cannot satisfactorily instruct full neuronal maturation of induced-newborn neurons in vitro. To overcome this limitation and enhance the neuronal differentiation of reprogrammed astrocytes, we combined here miR-124 with isoexasole-9 (ISX9) chemical compound known to possess neurogenesis-promoting properties (Xiang Li et al., 2015; Schneider et al., 2008) and have investigated their potential to instruct neuronal reprogramming of cortical astrocytes both in vitro and in vivo, focusing on the elucidation of the transcriptional and post-transcriptional mechanisms they control during reprogramming. Analysis of our RNA-seq data revealed that miR-124 is responsible for the reprogramming “switch” of astrocytes towards the neuronal fate by down-regulating genes with important regulatory roles in astrocytic function. We further identified the RNA binding protein Zfp36l1, implicated in mRNA decay (Lai et al., 2000), as a novel direct target of miR-124 by examining AGO-HITS-CLIP data obtained from mouse and human cortex and further found many neuronal specific targets of Zfp36l1 being up-regulated in miR-124-iNs, unveiling a novel miR-124/Zfp36l1 post-transcriptional mechanism with important implications during astrocytic reprogramming. On the other hand, our study revealed that the addition of ISX9 in the reprogramming medium promoted both the neurogenic conversion and the neuronal maturation of miR-124+ISX9-iNs enhancing the passage of reprogrammed cells through a Tbr2+ intermediate stage. In addition to its role during neuronal reprogramming and maturation, ISX9 was found to expand in vitro regional neuronal identity of reprogrammed cells by up-regulating at the transcriptional level many TFs related to other brain regions than the telencephalon, such as the midbrain and the hindbrain/spinal cord, by a yet unknown mechanism. miR-124 either alone or along with ISX9 is also potent to guide direct neuronal reprogramming of reactive astrocytes to iNs in vivo following cortical trauma, a

121 novel finding confirming the robust direct neuronal reprogramming action of the two
122 molecules in activated astrocytes in an in vivo setting. Interestingly the vast majority of in
123 vivo produced iNs exhibit deep-layer cortical identity, a fact verifying the regional barrier
124 imposed by the cortical microenvironment in neuronal sub-type specificity.

Results

miR-124 is potent to instruct reprogramming of postnatal cortical astrocytes to induced-immature neurons (iNs)

In order to study the potential of miR-124 to instruct neuronal reprogramming of astrocytes on its own, cultured postnatal day 3-5 (P3-5) mouse cortical astrocytes were transfected with the miR-124-3p mimic 3 times every two days and were supplemented with the antioxidants vitamin E for the first 3 days and ascorbic acid throughout the reprogramming protocol (**Fig.1A**). After 1 week (day7) nearly 35% of cells in culture exhibited multipolar morphology and were Tuj1+ as compared to scrambled miRNA control (sc-miRNA). Still, miR-124-iNs exhibited low differentiation potential and only about 19% Tuj1+ reprogrammed cells were detected at day14 of the reprogramming protocol (**Fig.1B, C**). The ability of miR-124 to instruct neurogenic reprogramming was further supported by quantitative expression analysis with RT-qPCR of several neurogenic transcription factors (TFs) at day7, where miR-124 overexpression induced the up-regulation of the mRNA levels of the proneural bHLH TFs Mash1 and to a lesser extend Neurog2 (**Fig.1D**), while it additionally up-regulated TFs related to both dorsal (Tbr2, Tbr1, Fezf2 and Cux1) (**Fig.1E**) and ventral telencephalon development (Gsx2, Dlx1) (**Fig.1F**). We also observed up-regulation of TFs related to neuronal differentiation (Sox4, Sox11, Hes6), however we failed to detect an up-regulation of NeuroD1 (**Fig.1G**), which is known to play a crucial role in neuronal reprogramming (Guo et al., 2014; Matsuda et al., 2019; Pataskar et al., 2016). Instead, miR-124 significantly reduced NeuroD1 mRNA levels, a finding possibly explained by the fact that NeuroD1 has been reported to be a developmental stage-specific direct target of miR-124 in Xenopus (Liu et al., 2011), which proposes a possible explanation for the low differentiation capacity of miR-124-iNs. Further analysis with immunofluorescence staining indicated that the majority of miR-124-iNs (nearly 80%) were Mash1+ and also exhibited low Tbr2 expression (nearly 70%), while only a small percentage of reprogrammed cells were positive for the ventral TF Gsx2 (**Fig.1H, I**), indicating that the Mash1-Tbr2 trajectory is most prominently activated in the majority of miR-124-iNs.

The neurogenic compound ISX9 greatly improves the miR-124-induced reprogramming efficiency and differentiation state of iNs

The observed down-regulation of NeuroD1 by miR-124 prompted us to supplement the reprogramming medium from day2 to day10 with the chemical compound ISX9, known to up-regulate NeuroD1 levels and enhance neuronal differentiation (Schneider et al., 2008). Indeed, the addition of ISX9 led to the acquisition of a more differentiated neuronal-like phenotype with a smaller soma and longer projections (**Fig.2A**) and significantly increased the percentage of Tuj1+ reprogrammed cells to 62% at day7, with an average of 38% of them being detected at day14 (**Fig.2B**). Importantly, ISX9 was potent to reverse the reduction of the mRNA levels of NeuroD1 induced by miR-124 (**Fig.2C**) and greatly enhanced the transcriptional levels of Neurog2 and Tbr2 peaking at day7, while it induced a moderate reduction in the mRNA levels of Mash1 (**Fig.2D**). Interestingly, ISX9 was not able to induce reprogramming of astrocytes on its own (sc-miRNA+ISX9) (**Suppl.Fig.1A**), despite inducing robust up-regulation of the mRNA levels of NeuroD1 (**Fig.2D**) and other neurogenic TFs (**Suppl.Fig.1B**) and to a small extend the protein levels of Mash1 and Tbr2 (**Suppl.Fig.1C, D**). Furthermore, the addition of ISX9 in the reprogramming medium along with miR-124 did not significantly affect neither the percentage of Mash1+/Tuj1+ iNs nor the percentage of Gsx2+/Tuj1+ iNs relative to miR-124 alone, but it moderately increased the percentage of Tbr2+/Tuj1+ iNs, as indicated by immunofluorescence analysis (**Fig.2E, F**). A step further, when we quantified the protein levels of Mash1 and Tbr2 by measuring their mean nuclear fluorescence intensity in miR-124-iNs and miR-124+ISX9-iNs at day7, we observed a significant enhancement of Tbr2 protein levels (**Fig.2G**) and a moderate down-regulation of Mash1 levels (**Fig.2H**) by the addition of ISX9, which are in agreement with the effect of ISX9 on the mRNA levels of these TFs and on Tbr2 up-regulation in particular.

These results led us to the inference that the addition of ISX9 in the reprogramming medium reinforces the passage of miR-124+ISX9-iNs through a Tbr2+ intermediate stage, which seems to be the main reprogramming route these iNs follow. Interestingly, the addition of ISX9 also significantly enhanced the expression of Insm1 (**Suppl.Fig.1E**), a key transcriptional regulator of intermediate progenitors (IPs) (Elsen et al., 2018), further supporting the notion that the iNs pass through an intermediate stage bearing molecular characteristics of endogenous IPs. Thus the combination of miR-124 with ISX9 seems to instruct neuronal reprogramming of astrocytes through activation of a transcriptional program that harbors

similarities with the molecular cascades governing cortical development and/or adult neurogenesis in the SVZ (Díaz-Guerra et al., 2013; Kwan et al., 2012).

miR-124+ISX9-iNs exhibit characteristics of mature, electrophysiologically active neurons

The majority of miR-124-iNs and miR-124+ISX9-iNs were positive for the cortical deep-layer TF Tbr1 at day14 (**Suppl.Fig.2A, B**). We observed mainly a moderate nuclear Tbr1 expression in miR-124-iNs, whereas miR-124+ISX9-iNs exhibited strong cytoplasmic Tbr1 expression, besides a moderate nuclear one (**Suppl.Fig.2A**). After 21 days in culture, nearly 80% of Tuj1+ miR-124+ISX9-iNs were also positive for the mature neuronal markers MAP2 and Synapsin1, exhibiting a mature neuronal-like morphology (**Fig3.A, B**), while miR-124-iNs at day21 did not exhibit signs of further maturation and only a small percentage of them were positive for MAP2 and Synapsin1 (**Fig.3B**).

In order to further establish the maturation state of miR-124-iNs and miR-124+ISX9-iNs we performed electrophysiological analysis with whole-cell voltage-clamp and current-clamp recordings at different time points from day15 to day27. In whole-cell configuration, rapidly inactivating inward Na^+ channels' (Na_V) currents and persistent outward voltage-gated K^+ channels' (K_V) currents were recorded in miR-124+ISX9-iNs (n=47 out of 80 analyzed cells) in response to depolarizing voltage steps (**Fig.3D, left panel**), while further application of TTX and TEA – selective Na_V and K_V blockers respectively – confirmed that the Na_V were responsible for the inward currents and K_V for the outward currents (**Fig.3D, middle and right panels**). On the other hand, miR-124-iNs lacked considerable amounts of K_V currents, while Na_V currents were sufficiently present (**Fig.3E**). Of note, only a small amount of K^+ currents were observed in the cells that were recorded before day21 (data not shown), while after day23, K^+ currents were observed in a large scale of miR-124+ISX9-iNs, which is in accordance with their ability to generate repetitive action potentials (APs) upon membrane depolarization and eventually after day26 and until later time points all the recorded miR-124+ISX9-iNs were capable of firing repetitive APs (n=21 cells out of 30 recorded cells) (**Fig.3F**). On the other hand, as expected, miR-124-iNs were not capable of firing APs due to low expression of K^+ channels which is not sufficient for AP formation (n=15 cells).

Further in our electrophysiological analysis, the majority (80%) of miR-124+ISX9-iNs (**Fig.3G**) and only a few miR-124-iNs (data not shown) were capable of responding to different concentrations of GABA early in the course of their maturation (day22), interestingly even before the appearance of APs for miR-124+ISX9-iNs, which is in compliance with the expression of GABA receptors in early stages of neuronal development (Luján et al., 2005).

Additionally, miR-124+ISX9-iNs were capable of responding to L-glutamate in a concentration dependent manner (**Fig.3H**), while L-glutamate-sensitive inward current was completely blocked after co-application of 100μM L-glutamate and 20μM CNQX, indicating the presence of AMPA/kainate receptors (**Suppl.Fig.2D**). Finally, we detected rare spontaneous electrical activity in a few mature miR-124+ISX9-iNs (day27) (**Fig.3I**).

miR-124 and ISX9 exhibit both unique and convergent molecular contributions in the reprogramming process to iNs

In order to better understand the molecular mechanism through which miR-124 alone or along with ISX9 contributes to the reprogramming process, we performed RNA-sequencing of miR-124-iNs and miR-124+ISX9-iNs at day7, using as control astrocytes obtained the initial day of the reprogramming (day1) and sc-miRNA transfected astrocytes at day7. The differential expression analysis was performed between day7 miR-124-iNs or miR-124+ISX9-iNs and day1 astrocytes (astro) (miR-124-iNs vs astro and miR-124+ISX9-iNs vs astro respectively), whereas the day7 sc-miRNA transfected astrocytes were used as the ultimate control for the analysis of miR-124 target genes (see next). We identified 4.252 differentially expressed genes (DEGs) in miR-124-iNs vs astro and 6.699 DEGs in miR-124+ISX9-iNs vs astro ($1 \leq \log_2(\text{fold change}) \leq -1$, FDR≤0,05).

A significant number of DEGs belonging to the GO terms: Glial cell differentiation, Gliogenesis, Astrocyte development, Generation of neurons, Neuron differentiation, Regulation of neuron differentiation, Neurotransmitter transport and Synaptic signaling were affected in miR-124-iNs vs astro and miR-124+ISX9-iNs vs astro, as shown in the heat map of **Fig.4A**. This analysis showed that miR-124 alone efficiently down-regulated a gene cluster enriched in astrocytic genes (Cluster I), with a small further contribution from ISX9. At the same time miR-124 up-regulated a gene cluster of neuronal specific genes (Cluster III) that was to a large extend further up-regulated by ISX9 supplementation, while ISX9 highly up-regulated a neuronal specific gene cluster (Cluster II) that was most exclusively expressed in miR-124+ISX9-iNs.

GO enrichment analysis of biological processes for the up-regulated DEGs of both miR-124-iNs vs astro and miR-124+ISX9-iNs vs astro further revealed that miR-124 alone up-regulated genes related to generation of neurons and neuron differentiation as well as to more specific neuronal functions mostly related to synaptic transmission (**Fig.4B in orange**), while the addition of ISX9 greatly enhanced the number of up-regulated genes related not only to the same GO terms, but also to more mature neuronal functions such as action potential,

axon development and subtype specific synaptic transmission (**Fig.4B in red**). Furthermore, enrichment analysis for the down-regulated DEGs of miR-124-iNs vs astro revealed that many of them were related to cell cycle, gliogenesis, and astrocyte differentiation (**Fig.4C**). Interestingly, this analysis revealed a strong effect of miR-124 in down-regulating components of many signaling pathways, including MAPK, PKB, canonical Wnt, TGF-β, BMP, Notch and JAK/Stat signaling pathways (**Fig.4C**), which are known to play important role in astrocytic identity and function (Acaz-Fonseca et al., 2019; Gross et al., 1996; Kang & Hébert, 2011; Yang et al., 2012).

Since reprogramming is a process that implicates great changes in the transcriptomic, post-transcriptomic and epigenetic landscape of trans-differentiating cells, we sought to identify the differentially expressed transcription factors (TFs), epigenetic factors (EFs) and RNA binding proteins (RBPs) in our datasets that could possibly drive the reprogramming process. Heat map analysis of astrocytic TFs (**Suppl.Fig.3A**) indicated that miR-124 alone potently down-regulated TFs related to astrocytic function such as Id1, Id3, Tcf4, Tcf7l1, Rbpj, Nfic, Zcchc24, Pparg, Nr3c1 and Tead1, while the addition of ISX9 exhibited only a small further contribution to their down-regulation (**Suppl.Fig.3A**). Interestingly, validation of many of those genes with RT-qPCR verified the observed trend and also indicated that ISX9 alone (sc-miRNA+ISX9) failed to down-regulate their mRNA levels (**Suppl.Fig.4B**). In parallel, heat map analysis of up-regulated neuronal specific TFs revealed that miR-124 alone led to the up-regulation of TFs related to telencephalon development such as Tox, Insm1, Foxo6, Scrt1, Rcor2, Rarb, Rxrg, Dlx5 and Sox21 (**Fig.4D**) along with TFs that we had already identified through prior RT-qPCR analysis (Mash1, Hes6, Sox4, Fezf2, Gsx2, Dlx1). Additionally, the supplementation with ISX9 increased the number of TFs implicated in telencephalic development, among which Eomes (Tbr2), Scrt2, Prdm8, Ovol2, Tfap2c, Tshz2, Lhx6 and Cux2 (**Fig.4D**). Surprisingly, we identified a rather large set of TFs highly up-regulated only following ISX9 addition that are presumed to be related to more ventral/caudal brain regions than the telencephalon, such as the retina, midbrain, hindbrain/spinal cord (**Fig.4D**), a finding posing the possibility that ISX9 expands region-specific neuronal identity at least at the transcriptional level. Validation of selected TFs/EFs expressed either in telencephalon (**Fig.4E**) or in midbrain (**Fig.4F**), hindbrain/spinal cord by RT-qPCR verified their observed up-regulation by the addition of ISX9 (**Fig.4G**).

Heat map analysis of differentially expressed RNA-binding proteins (RBPs) revealed that miR-124 was sufficient to down-regulate many RBPs expressed in astrocytes and other non-neuronal cells, such as the splicing factors Ptbp1, Snrpa1, Lgals3, Isy1, Ddx39 and Syf2, as

well as the mRNA decay proteins Zfp36, Zfp36l1, Zfp36l2 (**Suppl.Fig.3C**). In addition, miR-124 moderately up-regulated several neuron related RBPs, mostly relevant to mRNA splicing such as Elavl2, Elavl4, Nova1, Rbfox1, Rbfox2, Celf3, Nol3, Nol4 and Adarb1, while the addition of ISX9 induced further up-regulation of their mRNA levels and significantly increased the number of genes implicated in neuron specific splicing, editing or translation such as Aplp1, Celf4, Celf5, Celf6, Elavl3, Ern2, Esrp2, Rbfox3, Rbm11, Ssrm4 and Tdrd6 (**Suppl.Fig.3C**).

The analysis of differentially expressed EFs revealed that the addition of ISX9 had the major contribution in down-regulating EFs related to epigenetic transcriptional repression, such as the H3K9 methyltransferases Suv39h1 and Suv39h2, the histone deacylases Hdac5 and Hdac7, the components of repressor complexes Cbx5, Sap18 and Rbbp4, as well as the component of non-neuronal BAF complexes Dpf2 (**Suppl.Fig.3D**). On the other hand, miR-124 increased on its own the levels of several EFs related to epigenetic transcriptional activation, such as the H3K4 methyltransferase Kmt2c, the DNA demethylase Tet1, the chromatin remodeling factors Smarca1, Smarca2, Chd7, as well as the neuronal BAF (nBAF) complex component Ss18l1 (Crest), while ISX9 further contributed in up-regulating the brain specific chromatin remodeling factor Chd5, the neuronal TF which participates in BAF complexes Bcl11a, the nBAF complex components Actl6b and Dpf3 and the H3K4 methyltransferase Smyd3 (**Suppl.Fig.3D**).

The above observations led us to the conclusion that miR-124 over-expression is sufficient to induce the astrocytic reprogramming switch towards an immature cortical neuronal fate through down-regulation of many glial specific genes, many of which are implicated in different regulatory levels, such as the transcriptional, post-transcriptional, epigenetic and signaling pathway level. The addition of ISX9 on the other hand, greatly contributes to the enhancement of the neuronal-specific gene transcription related both to neuronal maturation and expansion of regional neuronal identity, by highly up-regulating neuronal specific TFs, EFs, RBPs and many genes related to neuron-specific functions.

The RNA-binding protein Zfp36l1 is a novel direct target of miR-124 with a key role in miR-124-induced cell fate switch

To get a closer insight into the post-transcriptional effects of miR-124 on the astrocytic transcriptome, we sought to determine the direct targets of miR-124 that could act as drivers of the reprogramming switch. Argonaute (AGO) HITS-CLIP (high-throughput sequencing of RNA isolated by crosslinking immunoprecipitation) experiments are

considered the avant-garde of high-throughput methodologies for the direct detection of miRNA targets on a transcriptome-wide scale. Therefore, we utilized publicly available AGO-HITS-CLIP data, performed in mouse brain cortex (Chi et al., 2009) to detect miR-124 binding sites. The analysis revealed 171 miR-124 direct targets that were also defined as down-regulated in the miR-124-iNs vs sc-miRNA RNA-Seq analysis (log_2(fold change)≤-1, FDR≤0,01). miR-124 targets were subsequently filtered to examine genes expressed in astrocytes, utilizing a published reference for expressed transcripts in distinct cell types of the mouse brain (Y. Zhang et al., 2014), ending up with 130 miR-124 direct target genes (**Fig.5A**).

Among these genes, a prominent target was the RNA-binding protein (RBP) Zfp36l1, which is implicated in the mRNA decay (Lai et al., 2000) and is highly expressed in cortical glial cells (Weng et al., 2019), cortical radial precursors (Weng et al., 2019; Yuzwa et al., 2017) and other non-neuronal cells (Carrick & Blackshear, 2007). miR-124 directly binds to the 3' UTR of Zfp36l1 transcript with perfect seed complementarity (7mer-M8 site) (**Fig.5B**). The interacting miRNA-gene pair was also examined in human species. Publicly available AGO-HITS-CLIP data from human motor cortex and cingulate gyrus tissues, were re-analyzed (Boudreau et al., 2014), revealing a conserved miR-124 binding site on the 3' UTR of ZFP36L1 human gene (**Fig.5B**).

The efficient down-regulation of Zfp36l1 by miR-124 was validated by RT-qPCR (**Fig.5C**), where interestingly ISX9 alone was not potent to down-regulate Zfp36l1 mRNA levels, further supporting our initial observation that ISX9 alone cannot instruct reprogramming of astrocytes to iNs, possibly by failing to down-regulate astrocytic fate genes.

Since Zfp36l1 acts by mediating degradation of its mRNA targets, we were interested in identifying Zfp36l1 mRNA targets, being up-regulated in our analysis. For this purpose, we combined two publicly available Zfp36l1 individual-nucleotide resolution CLIP-Seq data (iCLIP-Seq) from thymocytes (Vogel et al., 2016) and B lymphocytes (Galloway et al., 2016) and ended up with 619 Zfp36l1 direct targets that are up-regulated in miR-124-iNs vs sc-miRNA astro (log_2(fold change)≥1, FDR<0,05). GO enrichment analysis revealed that many of these genes are implicated in neurogenesis, neuron differentiation, telencephalon development, axonogenesis, dendritic morphogenesis and synaptic transmission (**Fig.5D**). Interestingly, many of them were also found to regulate transcription and RNA processing (**Fig.5D**), highlighting an important regulatory role for many Zfp36l1 targets, which could possibly have great impact on the reprogramming process. Among these targets we found neurogenic TFs, such as Tox, Tox3, Rcor2, Cux1, Hes6, Meis2, Mllt11, Ncoa2 and Zswim5, as well as the EFs also related to neurogenesis, Chd3, Chd7, Dnmt3a, Kmt2c, Ss18l1 (Crest) and

Tet1 (**Fig.5E**). Notably, we also identified as Zfp36l1 direct targets the neuronal RBPs Adarb1, Elavl4, Nova1 and Rbfox1 (**Fig.5E**). This constitutes a significant finding that delineates the neuronal RBPs' repression directly by Zfp36l1, being relieved upon miR-124-mediated Zfp36l1 down-regulation.

We subsequently examined the mRNA levels of the Zfp36l1 targets, Elavl4 and Nova1,as well as, of the other two neuron-specific RBPs of the neuronal Elav-like (nElavl) family, Elavl2 and Elavl3, with RT-qPCR, upon miR-124 overexpression in the presence or absence of ISX9. The analysis verified that miR-124, on its own, induced the up-regulation of Elavl4, Elavl2 and Nova1 and to a lesser extend of Elavl3 (**Fig.5F, G**). On the other hand, the addition of ISX9 enhanced the mRNA levels of all the tested genes, exhibiting the greatest impact on the mRNA levels of Elavl3 (**Fig.5F, G**).

miR-124 alone or in combination with ISX9 induces reprogramming of resident reactive astrocytes to iNs with deep-layer cortical identity *in vivo* following cortical mechanical trauma

To evaluate whether miR-124 alone or combined with ISX9 was also potent to drive cell fate conversion of resident reactive cortical astrocytes to iNs, we overexpressed miR-124 via lentiviral transfer into the mechanically injured cortex of mice. To this end we stereotaxically injected either one of the two lentiviruses, control LV-GFP and LV-miR-124-GFP, in order to transduce reactive astrocytes surrounding the cortical injury site, while 20 mg/kg ISX9 were systemically administered 2 days after viral injection for 5 consecutive days in a group of mice. We initially sacrificed a group of mice 6 days after viral administration (10 days after cortical trauma induction) to evaluate the original phenotype of transduced cells surrounding the injury site (**Suppl.Fig.4A**) and observed that the majority of them (68%) in both conditions were GFAP+ reactive astrocytes, while an average of 10% were NeuN+ neurons. The rest of the transduced cells were equally either Iba-1+ microglial cells or Olig2 oligodendrocytes (**Suppl.Fig.4B**). For all markers examined there were no statistically significant differences between LV-124-GFP and control LV-GFP, indicating that they are expected to transduce the same percentage of astrocytes and neurons upon injection into the cortical parenchyma. We, further on, examined the percentage of NeuN+ cells found amongst transduced GFP+ cells in the cortical parenchyma of animals administered with the two viral constructs, 3 weeks after the stereotaxic injection. The percentage of NeuN+/GFP+ transduced cells appeared to be significantly increased after 3 weeks in the animals that received the miR-124-overexpressing virus, but not the control virus (**Fig.6B, C**). In particular,

while approximately 10% of the transduced cells were NeuN+ in LV-GFP-injected animals, showing no significant difference between the 6 days and 3 weeks time points (p=0.104), 74% of the LV-miR-124-GFP-transduced cells were NeuN+ 3 weeks after the injection, showing significant difference between the two time points (LV-miR-124-GFP 6 days vs. LV-miR-124-GFP 3 weeks: p**=0.001037), indicating a strong potential of miR-124 to direct trans-differentiation of reactive astrocytes into iNs *in vivo*. The same effect was observed when the injection of LV-miR-124-GFP viral construct was accompanied by systemic administration of ISX9, where 71% of transduced cells were found to be NeuN+ (LV-124-GFP 6 days vs. LV-124-GFP+ISX9 3 weeks: p***=0.00012), while no difference was observed at 3 weeks after co-treatment of ISX9 in comparison to LV-miR-124-GFP injection alone (LV-124-GFP 3 weeks vs. LV-124-GFP+ISX9 3 weeks: p=0.737) (**Fig.6C, D**).

Further, overexpression of miR-124 either alone or along with ISX9 administration, appeared to drive the great majority of iNs towards a deep layer cortical identity, as the vast majority of the NeuN+ transduced cells after 3 weeks in both groups were also positive for the deep cortical layer marker Tbr1, with percentages reaching 98% in LV-miR-124-iNs and 88% in LV-miR-124-GFP + ISX9-iNs, with no significant difference between the two groups (p=0.15) (**Fig.6E, F**).

Discussion

In this study we have explored the potential of the brain enriched miRNA, miR-124, to instruct reprogramming of cortical astrocytes to induced-neurons (iNs) both in vitro and in vivo. miR-124 has been utilized in many reprogramming protocols for the conversion of fibroblasts (Ambasudhan et al., 2011; Birtele et al., 2019; Jiang et al., 2015; Victor et al., 2018; Yoo et al., 2011) or glial cells (Wohl & Reh, 2016) to iNs, however it has always been used in combination with other neurogenic factors, hindering the mechanistic insight into its reprogramming capacity and mode of action. In most cases, miR-124 has been used in combination with the neurogenic miRNAs, miR-9/9*, and the strong neuronal reprogramming potential of this combination has been elaborately studied at the transcriptomic and epigenetic level (Abernathy et al., 2017), while it has been further applied in combination with brain region specific TFs in order to generate sub-type specific iNs (Abernathy et al., 2017; Victor et al., 2014). Here we attempted to isolate miR-124 mechanism of action from that of other reprogramming co-factors and we provide evidence that miR-124 drives the trans-differentiation switch of cortical astrocytes to an immature iN phenotype of cortical identity, recapitulating pathways being activated during cortical neurogenesis and/or adult SVZ neurogenesis. Indeed, during their reprogramming, astrocytes pass from an intermediate stage expressing the TFs Mash1, Tbr2, Insm1, Tbr1, Cux1 and Fezf2, all being associated with neuronal commitment and differentiation along the course of embryonic (Kwan et al., 2012) and adult SVZ neurogenesis (Díaz-Guerra et al., 2013). This finding is in agreement with the role of endogenous miR-124 in embryonic cortical development (Maiorano & Mallamaci, 2009) and SVZ adult neurogenesis (Åkerblom et al., 2012; Cheng et al., 2009). Intriguingly, in our culture system we observed a significant down-regulation of the neuronal differentiation bHLH TF NeuroD1 after miR-124 over-expression, a finding that could be attributed to the fact that miR-124 has been reported to directly target NeuroD1 during an early stage of eye development in Xenopus, playing a temporal, developmental stage-specific anti-neurogenic role (Liu et al., 2011). We therefore hypothesized that this undesired blockage of NeuroD1 levels' increase might hamper the progression of the reprogramming and differentiation process of miR-124-iNs. For this, we employed the neurogenic compound ISX9 – that is known to up-regulate NeuroD1 (Schneider et al., 2008) – in our reprogramming protocol, in order to increase the levels of NeuroD1 and enhance both the reprogramming efficiency and the maturation state of iNs. ISX9 has been already used in chemical reprogramming protocols for the conversion of fibroblasts and astrocytes to iNs (Gao et al., 2017; Xiang Li et al., 2015) and has been shown

to mediate HDAC5 nuclear exit thus enhancing the de-repression of MEF2 and other neuronal specific genes, by increasing intracellular Ca^{2+} signaling (Schneider et al., 2008). Additionally, ISX9 has been shown to enhance the differentiation of iPSC-derived neurons from patients with juvenile or adult-onset Huntington's disease, indicating that it also possesses a neuronal differentiation and maturation-promoting activity (Lim et al., 2017). Indeed, the addition of ISX9 greatly improved the reprogramming efficiency and differentiation status of miR-124+ISX9-iNs, while our analysis revealed that ISX9 enhanced, as expected, the levels of NeuroD1, as well as, the Neurog2 – Tbr2 transcriptional cascade, reinforcing the passage of miR-124+ISX9-iNs through a Tbr2+ intermediate stage, that harbors molecular characteristics of endogenous IPs. Interestingly, despite a robust up-regulation of NeuroD1 levels, as well as, many other neuronal TFs by ISX9 alone, control sc-miRNA+ISX9-treated astrocytes failed to undergo reprogramming. NeuroD1 has been extensively reported to possess a strong reprogramming capacity towards the neuronal fate (Guo et al., 2014; Matsuda et al., 2019; Rivetti Di Val Cervo et al., 2017) exhibiting pioneer factor activity (Pataskar et al., 2016), however we hypothesize that very high levels of NeuroD1 are required to inflict these effects, since these studies have used viral-mediated NeuroD1 overexpression. The addition of ISX9 in our reprogramming protocol may not lead to the required levels of NeuroD1 in order to exert its pioneer reprogramming activity. Interestingly, ISX9 was potent to convert highly malignant astrocytes bearing mutations in genes important for the astrocytic state into Tuj1+ cells, also indicating that astrocyte-specific barriers need to be overcome first in order for ISX9 to induce the neuronal fate (Ling Zhang et al., 2011).

Our RNA-Seq analysis highlighted the importance of miR-124 over-expression in the direct or indirect down-regulation of astrocytic genes with significant regulatory role in astrocytic identity and function, among which TFs, RBPs, EFs and components of signaling pathways, in support of the notion that astrocytic identity barriers need to be repressed before the induction of a neurogenic cell fate during the reprogramming process and in accordance with the documented role of miR-124 in controlling the choice between astrocytic and neuronal fate during neuroblastoma and neural stem cell (NSC) differentiation (Neo et al., 2014). Conversely, the addition of ISX9 had a small contribution in the repression of astrocytic genes and we propose here that this might be the reason for the inability of this chemical compound to confer the reprogramming switch when added on its own. Our analysis of the direct miR-124 targets utilizing AGO-HITS-CLIP data from mouse cortex (Chi et al., 2009) revealed the RBP Zfp36l1 as a novel target of miR-124. Of note, we also verified

the miR-124/Zfp36l1 interaction in human bearing the same binding site, by analyzing AGO-HITS-CLIP data from human motor cortex and cingulate gyrus (Boudreau et al., 2014), highlighting the importance of this conserved interaction during mammalian brain evolution. Many studies over the years have identified several direct targets of miR-124 with important regulatory role in neurogenesis, acting at the transcriptional level, such as the TFs Sox9 (Cheng et al., 2009) and Lhx2 (Sanuki et al., 2011), the epigenetic level, such as the components of the REST repressor complex, Scp1 (Visvanathan et al., 2007) and Rcor1 (Baudet et al., 2012; Volvert et al., 2014), the component of the PRC2 complex Ezh2 (Neo et al., 2014) and the component of the BAF complex BAF53a (Yoo et al., 2009a), as well as at the post-transcriptional level, such as the RBP involved in alternative splicing Ptbp1 (Makeyev et al., 2007). Here, we report for the first time that miR-124 is directly implicated in the regulation of another process mediated by RBPs, the mRNA decay. Zfp36l1 is a member of the Zfp36 family of proteins along with Zfp36 and Zfp36l2, which act by binding to AU rich elements (AREs) in the 3'UTR of their mRNA targets mediating their destabilization (Lai et al., 2000). Furthermore, Zfp36l1 is expressed in cortical radial precursors (DeBoer et al., 2013; Weng et al., 2019; Yuzwa et al., 2017), cortical glial cells (Weng et al., 2019), as well as non-neuronal cells (Carrick & Blackshear, 2007; Chen et al., 2015). We next sought to identify targets of Zfp36l1 being up-regulated in our analysis and for this we examined data from Zfp36l1-iCLIP-Seq experiments in thymocytes (Vogel et al., 2016) and B lymphocytes (Galloway et al., 2016). Although our analysis was restricted to a transcriptome not relevant to the astrocytic transcriptome, we identified a rather large number of Zfp36l1 targets being up-regulated in miR-124-iNs that exhibit significant regulatory role in neurogenesis and neuronal differentiation, underlining a novel miR-124/Zfp36l1 interaction with critical impact on the reprogramming process that mediates the de-repression of neuronal mRNA processing, apart from the well characterized miR-124/Ptbp1 circuitry (Makeyev et al., 2007; Yeom et al., 2018). Interestingly, the ARE-dependent mRNA decay seems to be regulated by other neurogenic miRNAs as well, since the close paralog of Zfp36l1, Zfp36, is targeted by miR-9 (Dai et al., 2015), suggesting another combined action of those two neurogenic miRNAs in the regulation of Zfp36 family members, in order to counteract the destabilization of neuronal mRNAs during neurogenesis. Of note, our analysis identified the neuron-specific RBPs Elavl4/HuD, Nova1 and Rbfox1 as targets of Zfp36l1, while Zfp36 has been reported to directly target Elavl2/HuB, Elavl3/HuC and Nova1 (Dai et al., 2015), implying a complementary and synergistic role of Zfp36l1 and Zfp36 in repressing neuron-specific RBPs in non-neuronal

cells. Furthermore, our analysis highlighted the implication of miR-124 in the regulation of ARE-containing neuronal mRNAs as a contributing factor in the induction of the neurogenic switch from the destabilizing Zfp36 family proteins to the stabilizing nElavl proteins (Pascale et al., 2008; Scheckel et al., 2016). Importantly, the expression of Zfp36l1 is spatially enriched in the radial precursors of the ventricular zone (VZ) (DeBoer et al., 2013; Weng et al., 2019; Yuzwa et al., 2017) and substantially decreases during neocortical development (DeBoer et al., 2013), while Elavl4/HuD is expressed early in the course of cortical neurogenesis in proliferating neuronal progenitors of the intermediate and outer VZ driving them to exit the cell cycle (Akamatsu et al., 2005), unveiling a possible endogenous role of this novel miR-124/Zfp36l1/Elavl4 axis during cortical neurogenesis, which deserves further exploration.

Interestingly, the up-regulation of the nElavls' mRNA levels seems to be a point of convergence between miR-124 and ISX9, since the addition of ISX9 significantly enhanced the moderate up-regulation of Elavl3 induced by miR-124 alone and further contributed in the up-regulation of Elavl2 and Elavl4, supporting its neuronal differentiation role in the reprogramming process. Along this line, the supplementation of ISX9 greatly enhanced the transcription of neuronal specific regulatory TFs, RBPs and EFs, as well as other genes related to neuronal maturation and subtype specific signaling. To this end our analysis revealed that the addition of ISX9 significantly increased the levels and the number of TFs related to telencephalon development and/or adult OB neurogenesis, further reinforcing the cortical identity of iNs already initiated by miR-124. Surprisingly, ISX9 also up-regulated a large set of TFs related to the development of other non-telencephalic brain regions such as the midbrain and the hindbrain/spinal cord. However, the mechanism of the observed here ISX9-mediated up-regulation of ventral/caudal TFs still remains elusive. Interestingly, ISX9 has been shown to affect the epigenetic landscape by increasing H3/H4 acetylation through an ERK1/2-mediated activation of the histone acetyl-transferase p300 in pancreatic β-cells (Dioum et al., 2011), suggesting that a possible epigenetic mechanism may be responsible for this observed up-regulation, a hypothesis that needs to be further explored.

Here we also demonstrate that miR-124 is capable of directly converting reactive cortical astrocytes surrounding a mechanically-induced trauma to iNs of deep-layer cortical identity. Brain injury is known to facilitate in vivo reprogramming, making astrocytes more plastic by activating low levels of NSC genes' expression (Götz et al., 2015). In vivo reprogramming of reactive astrocytes to neuronal precursors and iNs has been achieved following forced expression of TFs among which Sox2 (Niu et al., 2013), Neurog2 (Grande et al., 2013),

NeuroD1 (Guo et al., 2014; Rivetti Di Val Cervo et al., 2017) and Nurr1/Neurog2 (Mattugini et al., 2019), in some cases combined with anti-apoptotic and/or anti-oxidant treatment to enhance survival (Gascón et al., 2016). However, it is the first time that miR-124 is shown to reprogram reactive astrocytes to NeuN+ iNs with a high efficiency of 74%. By contrast to the in vitro situation, co-administration of ISX9 didn't significantly further enhance miR-124-induced reprogramming efficiency in vivo, as estimated 3 weeks after the infliction of the trauma, a finding implying the strong effect of the surrounding micro-environment in supporting miR-124-induced neuronal conversion. Indeed, proinflammatory cytokines like TNF, and growth factors such as EGF, FGF2 and SHH present in the injured cortex have been reported to facilitate the neurogenic conversion of astrocytes (Gabel et al., 2016; Grande et al., 2013; Sirko et al., 2013). Of note, another possible explanation for the enhanced miR-124 reprogramming potency in the in vivo setting apart from the influence of the microenvironment, is the lentiviral-mediated miR-124 overexpression strategy being used, which results in sustained but lower miR-124 levels in transduced cells, leading to differential regulation of miR-124 targets. Therefore it could be possible that NeuroD1 mRNA levels, being targeted by the miR-124-3p mimics overexpression in vitro, are partially rescued in vivo due to lower levels of miR-124 expression in transduced cells.

Importantly following either miR-124 or miR-124+ISX9 overexpression all iNs possess a deep-layer cortical identity expressing Tbr1. Taking into account the fact that the injury has been performed in a deep cortical area just above the corpus callosum, this observation indicates that, region-specific neuronal identity barriers are imposed to newly produced iNs by the surrounding cortical microenvironment. This comes in accordance with recent findings unravelling the existence of layer-driven neuronal identity during in vivo astrocytic reprogramming to iNs (Mattugini et al., 2019).

Our in vivo findings point to an even stronger reprogramming capacity of miR-124 than the one observed in vitro, opening the possibility for its use in therapeutic protocols in vivo with minimal support by other neurogenic or anti-inflammatory/anti-oxidant factors. It would be interesting to explore in the future if non viral approaches for the delivery of miR-124-3p mimics can be as effective as the viral approaches concerning their reprogramming efficiency.

Materials and Methods

Primary cultures of postnatal cortical astrocytes

Primary postnatal astrocytic cultures from P3-P5 mice were prepared as previously described (Aravantinou-Fatorou et al., 2015). Briefly, the cerebral cortexes from 2-3 P3-P5 C57BL/6 mice were collected in ice cold HBSS (Invitrogen), the tissue was washed three times with HBSS and digested with 0,4% trypsin (Sigma) and 10 μg/ml DNAse (Sigma) for 5 min at 37°C. After digestion cells were mechanically dissociated, centrifuged for 5 min at 850 rpm (120 g), resuspended in DMEM 4,5 g/lt glucose (Invitrogen) containing 10% FBS (Invitrogen), 1% Penicillin/Streptomycin (Pen/Strep) (Sigma) and placed in a T75 flask. When culture reached confluence (usually after 7-10 days), the flask was shaken in a horizontal shaker at 200-250 rpm for 16-20 h, in order to obtain a pure astrocytic culture, free from neurons, oligodendrocytes and microglia. The remaining cells were digested with 0,25% trypsin-EDTA (Invitrogen) for 5 min at 37°C, centrifuged at 850 rpm, resuspended in fresh DMEM 4,5 g/lt glucose 10% FBS, 1% Pen/Strep and divided in two new T75 flasks. Half of the medium was changed every two days.

In vitro reprogramming protocol

For reprogramming of astrocytes to induced-neurons, 40.000 astrocytes were seeded in 10 mm coverslips coated with 20 μg/ml poly-L-ornithine (PLO) (Sigma) overnight and 5 μg/ml laminin for 3 h at 37°C (Sigma). Once cells reached>90% confluence (usually after 1-2 days) they became transfected with 80 pmol miR-124-3p mimics or sc-miRNA mimics (negative control) (Dharmacon) using Lipofectamine 2000 (Invitrogen) according to manufacturer's instructions (day1). The next day the astrocytic medium (DMEM 4,5 g/lt glucose, 10% FBS, 1% Pen/Strep) was replaced with the reprogramming medium: Neurobasal (Invitrogen) supplemented with 1X B27 (Invitrogen), 1X GlutMAX (Invitrogen), 20 μM vitamin E (Sigma) and 200 mM ascorbic acid (Sigma). The same process of transfection was repeated twice at day3 and day5. Vitamin E was added to the medium until day4, while ascorbic acid was added throughout the reprogramming protocol. At day7 the reprogramming medium was changed to the neuronal differentiation medium: Neurobasal supplemented with 1X B27, 1X GlutMAX, 20 ng/ml BDNF (R&D Systems), 0,5 mM cAMP (Sigma) and 200 mM ascorbic acid. In the miR-124+ISX9-reprogrammed cells, 10 μM of ISX9 chemical compound (Tocris) were added from day2 to day10. All the mediums added to the reprogrammed cells were pre-conditioned for 24 h in a confluent astrocytic culture.

RT-qPCR analysis

For the RT-qPCR analysis experiments, total RNA was extracted using the Nucleospin miRNA kit (Macherey-Nagel) and 500-800 ng of total RNA were used for cDNA synthesis with the Superscript II reverse transcriptase (Invitrogen) according to manufacturer's instructions. Quantitative real time PCR was performed using SYBR Select Master Mix (Applied Biosystems). The primers used are listed in **Table 1**. Each sample was analyzed in triplicates, gene expression was calculated using the ΔΔCt method and all the results were normalized to β-actin expression. Relative expression was estimated setting the values of sc-miRNA transfected astrocytes to 1. All experiments were performed at least in triplicates.

Immunocytochemistry

Cells were washed once with PBS and then fixed with 4% paraformaldehyde for 20 min at room temperature. Afterwards, cells were washed three times with PBS and blocked with 5% normal donkey serum (NDS) (Merck-Millipore), 0,1% Triton X-100 in PBS for 1 h at room temperature. For nuclear staining, cells were permeabilized with 0,25% Triton X-100 in PBS for 10 min at room temperature and washed three times with PBS prior to blocking. Next, cells were incubated with primary antibodies, diluted in 1% NDS, 0,05% Triton X-100 in PBS overnight at 4°C. The next day, cells were washed three times with PBS and incubated with secondary antibodies diluted in 1% NDS, 0,05% Triton X-100 in PBS for 2 h at room temperature. The nuclei of the cells were stained with ProLong Gold Antifade Reagent with DAPI (Cell Signalling). The following primary antibodies were used in this study: mouse anti-Tuj1 (Covance, 1:600), chicken anti-Tuj1 (Millipore, 1:1000), mouse anti-MAP2 (Millipore, 1:200), rabbit anti-Synapsin1 (Abcam, 1:200), rat anti-Mash1 (R&D Systems, 1:100), rabbit anti-Tbr2 (Abcam, 1:200), rabbit anti-Gsx2 (Millipore, 1:400). The secondary antibodies used in this study were Alexa Fluor 546-, Alexa Fluor 488- and Alexa Fluor 647-conjugated secondary antibodies (Life Technologies). Images were acquired using Leica TCS SP8 confocal microscope (LEICA Microsystems).

Measurement of mean fluorescence intensity

We developed a Fiji macro which performs mean intensity measurement of Tbr2 and Mash1 staining inside the cell nuclei in maximum intensity projections. Initially automatic detection of nuclei was performed using the Otsu method andTuj1+ cells were selected based on their mean intensity value above a user-defined threshold of 40 followed by a manual validation according to cell morphology. Tbr2 and Mash1 mean intensity was measured for Tuj1- and

Tuj1+ cells. For each experiment measurements from at least 200-300 cells were obtained for each condition.

Electrophysiology

For whole-cell recordings iNs plated in PLO-laminin coated coverslips were used for electrophysiological experiments beginning at day15 and up to day27 of the reprogramming protocol. The coverslips with the cells were placed onto a recording chamber and viewed using an Olympus CKX41 microscope with a 40x lens. The cells were bathed in a solution containing: 140 mM NaCl, 2,8 mM KCl, 2 mM $CaCl_2$, 4 mM $MgCl_2$, 10 mM Glucose, and 20 mM HEPES. For whole-cell recordings we used a capillary glass with Filament (Sutter instrument) to fabricate low resistance recording pipettes (~5 MΩ) and filled with: 140 mM KCl, 2mM $CaCl_2$, 2mM $MgCl_2$, 2mM Mg-ATP, 5 mM EGTA and 10 mM HEPES. Osmolarity and pH of all solutions were adjusted appropriately before experiments. Data were acquired at room temperature (22–24°C) using an EPC9 HEKA amplifier and an ITC-16 acquisition system with a patch master software (HEKA). Data analysis was carried out using OriginPro8. **Voltage protocols:** The membrane of the cells was held at a holding potential of -70 mV and step depolarizing pulses were applied. Depolarization steps were applied for 50 msec in 10 mV increments from -80 mV to +50 mV with a sweep interval time of 1 sec and a sweep duration of 500 ms. Each depolarizing pulse was proceeded by a hyperpolarizing step to -120 mV. **Current protocols:** Cells we held at their resting membrane potential (0 pA) and depolarizing current steps from -20 pA to 200 pA from a holding current of 0 pA were applied.

RNA-Seq experiment and bioinformatic analysis

For the RNA-Seq experiment, the following samples were prepared in 3 biological replicates: astrocytes (day1), sc-miRNA-transfected astrocytes (day7), miR-124-iNs (day7) and miR-124+ISX9-iNs (day7). Total RNA was extracted using the Nucleospin miRNA kit (Macherey-Nagel) according to manufacturer's instructions. Libraries were prepared with TruSeq RNA Library Prep Kit v2 (Illumina) before 75c single-end sequencing in an Illumina NextSeq 550 sequencer. Raw libraries were quality checked and preprocessed using FastQC (https://www.bioinformatics.babraham.ac.uk/projects/fastqc/). Mapping of reads against the Human Transcriptome (v.GRCh38.rel79) and transcript abundance estimation on Transcripts Per Million (TPM) values was performed using kallisto (Bray et al., 2016). Analysis of differential expression, interpretation and visualization was subsequently

668 performed using kallisto-compatible Sleuth tool (Pimentel et al., 2017) and R-base functions.
669 Gene ontology (GO) enrichment analysis was performed using the Gene Ontology Panther
670 Classification System (http://pantherdb.org/). High throughput sequencing data have been
671 deposited in the European Nucleotide Archive under Study accession PRJEB38603, and will
672 be made publicly available upon acceptance of the manuscript as a Paper in Press.

673 **Analysis of AGO-CLIP-Seq data**

674 AGO-HITS-CLIP datasets, performed in mouse brain cortex tissue (P13 neocortex, 5
675 replicates) and human brain tissues (motor cortex, cingulate gyrus) from 2 individuals, were
676 retrieved from the publications (Chi et al., 2009) and (Boudreau et al., 2014)
677 respectively. Raw libraries were quality checked using
678 FastQC (www.bioinformatics.babraham.ac.uk/projects/fastqc/), while adapters/
679 contaminants were detected utilizing an in-house developed pipeline and the Kraken suite
680 (Davis et al., 2013). Pre-processing was performed with TrimGalore (Krueger, 2015) and
681 Cutadapt (Martin, 2011). CLIP-Seq libraries were aligned against the reference genomes, i.e.
682 GRCh38 and mm10 assemblies for human and mouse respectively, with GMAP/GSNA (Wu &
683 Nacu, 2010) spliced aligner, allowing up to 2 mismatches. microCLIP CLIP-Seq-guided model
684 (Paraskevopoulou et al., 2018) was utilized to identify binding events for the expressed
685 miRNAs. In case of multiple replicates (i.e. mouse brain cortex) a miRNA binding event had
686 to be present in at least two replicates to be considered as valid. Top expressed miRNAs
687 were retrieved from the relevant publications. Human and mouse transcriptomes were
688 compiled from ENSEMBL v96 (Cunningham et al., 2019) to annotate the retrieved miRNA
689 binding events. Identified miRNA binding sites residing on 3' UTR regions were retained and
690 subsequently filtered to preserve only genes expressed in astrocytes. A list of ~10,000 genes,
691 expressed in astrocytes, with FPKM ≥ 2, was retrieved from a reference publication and
692 retained for analysis (Y. Zhang et al., 2014).

693 **Lentiviral production**

694 For lentiviral in vivo transduction, VSV-G (Vesicular Stomatitis Virus–Glycoprotein)–
695 pseudotyped lentiviruses were used either for the over-expression of miR-124 along with
696 GFP or as control expressing only GFP. More specifically, for lentiviral particles' production,
697 HEK 293T cells cultured in 10-cm Petri dishes at a 50-60% confluence were co-transfected
698 with 10 μg lentiviral plasmid expressing miR-124-1 precursor under the CMV promoter and
699 GFP under the EF1 promoter (SBI System Biosciences) or 10 μg lentiviral plasmid expressing

GFP under the CMV promoter (SBI System Biosciences) and the packaging plasmids pVSV-G (3,5 μg), MDL (6,5 μg), and RSV-REV (2,5 μg) (kindly provided by Dr. Matsas lab) with calcium phosphate. The following day the culture medium was replaced with fresh one, the supernatant containing the lentiviral particles was collected 48 h and 72 h (second harvest) after transfection and concentrated by ultracentrifugation at 25.000 rpm (80.000 x g) for 2 h at 4°C.

Cortical trauma, viral injection, and ISX9 administration

This study was carried out in strict compliance with the EuropeanDirective 2010/63/EU and the Greek National Law 161/91 for Useof Laboratory Animals, according to FELASA recommendations for euthanasia and the National Institutes of Health Guide for Care andUse of Laboratory Animals. All protocols were approved by the Animal Care and Use Committee of the Hellenic Pasteur Institute (Animal House Establishment Code: EL 25 BIO 013). License No 2585/29-5-18 for the experiments was issued by the Greek authorities of the Veterinary Department of the Athens Prefecture. The manuscript was prepared in compliance with the ARRIVE guidelines for reporting animal research.

Adult male and female FVB mice (8-16 weeks old) were deeply anaesthetized using inhalable isoflurane, and positioned in a stereotaxic apparatus. The dorsal surface of the skull was exposed through a midline incision and a burr hole was drilled at the following coordinates: antero-posterior (AP) -1,00 mm, caudal to bregma; lateral (L) 1,0 mm to the midline (Franklin and Paxinos, 2001). A 26-gauge needle was inserted into the brain parenchyma in a depth of 0,9 mm from the surface of the brain to create a trauma in the cortex, avoiding the structure of hippocampus. The inserted needle was moved along the anterior-posterior axis between positions (AP) -1,1 and -0,9 to widen the trauma. The skin was sutured, a local analgesic creme containing 2,5% lidocain and 2,5% prilocain was applied and the animals were kept warm until they were fully awake. Viral injection took place 4 days after the cortical trauma. A 10 μl Hamilton syringe (Hamilton) with a 26-gauge needle was slowly inserted into the brain tissue at coordinates (AP) -1,1 mm, (L) 1,0 mm, and (V): 1,0 mm, from the same burr hole on the skull and 2 μl of lentiviral concentrate was injected at a rate of 0,5 μl/min. The needle was left in position for 5 min after each injection and then withdrawn gently. A second viral injection was repeated at coordinates (AP) -0,9 mm, (L) 1,0 mm, and (V): 1,0 mm with similar procedures, and the then the surgery was completed as described. A group of animals was injected with the lentivirus LV-miR-124-GFP (group LV-124), and another one with the control lentivirus LV-GFP (group LV-GFP). A subgroup of the LV-124 group received

intraperitoneally 20 mg/kg of ISX9 (Tocris) diluted in (2-Hydroxypropyl)-β-cyclodextrin (Sigma) (ISX9 concentration: 2 mg/ml in 30% (2-Hydroxypropyl)-β-cyclodextrin (Sigma) diluted in sterile ddH_2O) once a day, for 5 consecutive days, beginning 48 h after lentiviral injection. Animals were sacrificed 6 days or 3 weeks after viral injection.

Tissue Preparation, Histology, and Immunohistochemistry

For histology, mice were deeply anaesthetized by inhaling isoflurane, and perfused with 4% paraformaldehyde (PFA) via left cardiac ventricle. The brains were removed, post-fixed in 4% PFA overnight, and then cryoprotected in 20% sucrose overnight. Tissues were then frozen in -20°C isopentane and cut into 20 µm-thick coronal sections on a cryostat (Leica CM1900), collected on silane-coated slides and stored at -20°C. For detection of specific antigens with immunofluorescence, sections were left for 15 min in room temperature, washed in PBS, and blocked with 5% normal goat or donkey serum (Merck-Millipore) in PBT (0.1% Triton X-100/PBS) for 1 h. Incubation with primary antibodies took place overnight at 4oC. Primary antibodies to assess transduced cell identity used were: chicken polyclonal anti-GFP (Abcam, 1:1000) to detect the transplanted cells, mouse monoclonal anti-neuronal nuclei (NeuN) (Merck-Millipore, 1:300) to identify mature neurons, rabbit polyclonal anti-glial fibrillary acidic protein (GFAP) (Dako, 1:600) to detect astrocytes; rabbit polyclonal anti-oligodendrocyte transcription factor 2 (Olig2) (Merck-Millipore, 1:200),rabbit polyclonal anti-ionized calcium-binding adapter 1 (Iba-1) (Wako, 1:600) for detection of microglia and rabbit polyclonal anti-Tbr1 (Abcam, 1:250) for detection of deep layer cortical neurons. Following incubation with primary antibodies, sections were washed with PBS and incubated for 2 h with the appropriate secondary antibodies conjugated with AlexaFluor 488 (green), 546 (red), or 647 (blue) and TO-PRO-3 (Molecular Probes) for nuclei staining. Finally, sections were washed and coverslipped with Mowiol (Calbiochem). Images were acquired using Leica TCS SP8 and Leica TCS-SP5II confocal microscopes (LEICA Microsystems).

Quantification of Immunofluorescence for in vivo analysis

For each animal and each immunofluorescence staining, cell counting was performed on brain sections collected at 240 lm intervals across the whole antero-posterior extent of the hippocampus (bregma-0,5mm up to -2,5mm). For estimation of the ratio of transduced cells that have a specific phenotype, images for GFP+ cells found in each set of sections were acquired and co-localization with cell type-specific markers was evaluated by an observer “blind” to treatment group and time point. All GFP+ cells found in the cortex within these

765 sections were imaged and analyzed. Representative confocal images shown in **Fig.6** and
766 **Suppl.Fig.4** are obtained from coronal sections, antero-posterior positions between 21.3 and
767 22.2 relative to bregma.

768 **Statistical analysis**

769 All in vitro quantified data are presented as average ± SD, unless otherwise indicated. Two-
770 tailed Student t-test was used to calculate statistical significance with p values, where p
771 values less than 0,05 ($p<0,05$) were considered indicative of significance. In vivo data were
772 assessed using a one-way analysis of variance (ANOVA). When interactions were detected,
773 group comparisons were performed using a two-sample assuming unequal variances test.
774

775 **Acknowledgments**

776 This work was financially supported by: 'BIOIMAGING-GR: A Greek Research Infrastructure
777 for Visualizing and Monitoring Fundamental Biological Processes (MIS 5002755)' Grant,
778 funded by the Operational Program "Competitiveness, Entrepreneurship and Innovation"
779 (NSRF 2014-2020) co-financed by Greece and the European Union (European Regional
780 Development Fund); Fondation Sante Grant 2017-2018 and ARISTEIA-II 'Astro-Rep' 3713
781 Excellence Grant of the Greek Ministry of Education, awarded to DT. We also acknowledge
782 funding from the Stavros Niarchos Foundation Grant to the Hellenic Pasteur Institute, as part
783 of the Foundation's initiative to support the Greek Research Center ecosystem and KRIPIS
784 action under the Operational Strategic Reference Framework 2014–2020/MIS 5002486.
785

786

787

788

789

790

791

792

793

794 **Table 1:** Sequences of the primers used in this study

Gene	Forward primer	Reverse primer
Mash1	TCTCCGGTCTCGTCCTACTC	CAAAGTCCATTCCCAGGAGA
Neurog2	GTCCCCATACAGCTGCACTT	CAGGTGAGGTGCATAACGGT
Tbr2	CACCCAGAATCTCCTAACACTG	AGCCTCGGTTGGTATTTGTG
Tbr1	TCCAGACGTTCACTTTTCCG	CCCGTGTAGATCGTGTCATAG
Cux1	AGCAGAGACTTTAAGGGAACAG	GCAGCCAACTCTACTTCTAGG
Fezf2	TTTGTGGCAAAGGCTTTCAC	TCTTGTCGTTGTGGGTGTG
Gsx2	GATTCCACTGCCTCTCCATG	CGGGACAGGTACATATTGGAAG
Dlx1	CAGTTCCGTGCAGTCCTAC	ATTGTCCTGGGTTTACGGATC
Sox4	GAACGCCTTTATGGTGTGGT	GAACGGAATCTTGTCGCTGT
Sox11	CCCTGTCGCTGGTGGATAAG	GGTCGGAGAAGTTCGCCTC
Hes6	TACCGAGGTGCAGGCCAA	AGTTCAGCTGAGACAGTGGC
NeuroD1	TTGAAGCCATGAATGCAGAG	TCTTGGGCTTTTGATCATCC
Scrt1	AATCATGCCCAGGTCCTTC	CCACGTAGTCACTGAGGTATC
Lhx6	GACACCATGATCGAGAACCTC	CAATTGCTCTGCGGTGAAG
Chd5	ATCTACGAAATCTGGCACCG	CCCTTGTGGATCTCAGACTTG
En1	CTACTCATGGGTTCGGCTAAC	TCTTTAGCTTCCTGGTGCG
Foxa1	AGGGTTGGATGGTTGTGTC	AGGCCGGAGTTCATGTTG
Lmx1b	CGGGATCGGAAACTGTACTG	AGCAGAAACAGCCCAAGTG
Hoxc4	CAAGCAACCCATAGTCTACCC	AACTCTTTCTCTAATTCCAGGACC
Phox2a	TCCCTTCTCTGGAGTTCTGTC	GATAATGCCAGGTCCAGAAGG
Elavl2	AATAACAGGGCAGAGCTTGG	TCTGATTGAGGCTGAGCTTG
Elavl3	GGTTCGGGATAAGATCACAGG	CAGAACTGGGACGTGCATAG
Elavl4	AGAATCCTGCAAACTCGTGAG	ATGGTTTTGGTCTGGAGTCTG
Nova1	GCTGGCTACCTCTGGATCAT	TGGGATGCCATTTAGCTTGC
Zfp36l1	CACACCAGATCCTAGTCCTTG	CTGGGAGTGCTGTAGTTGAG
Zfp36	TCTCTTCACCAAGGCCATTC	GAGTCCGAGTTTATGTTCCAAAG
Rbpj	TCCCAAAACCCGGATAACC	TTTCGCATAGCTTCCCTAGTG
Tcf7l1	CTACAGCAACGACCACTTCTC	GGTAATACGGTGACAGCTCAG
Tcf4	CACAAACCATTACAGCACCTC	GTGTGGTCAGGAGAATAGATCG
Nfic	GGACGGAAGACATAGAAGGAG	GGGCTGTTGAATGGAGATTTG

795

Bibliography

Abernathy, D. G., Kim, W. K., McCoy, M. J., Lake, A. M., Ouwenga, R., Lee, S. W., Xing, X., Li, D., Lee, H. J., Heuckeroth, R. O., Dougherty, J. D., Wang, T., & Yoo, A. S. (2017). MicroRNAs Induce a Permissive Chromatin Environment that Enables Neuronal Subtype-Specific Reprogramming of Adult Human Fibroblasts. *Cell Stem Cell*, *21*(3), 332-348.e9. https://doi.org/10.1016/j.stem.2017.08.002

Acaz-Fonseca, E., Ortiz-Rodriguez, A., Azcoitia, I., Garcia-Segura, L. M., & Arevalo, M. A. (2019). Notch signaling in astrocytes mediates their morphological response to an inflammatory challenge. *Cell Death Discovery*. https://doi.org/10.1038/s41420-019-0166-6

Akamatsu, W., Fujihara, H., Mitsuhashi, T., Yano, M., Shibata, S., Hayakawa, Y., Okano, H. J., Sakakibara, S. I., Takano, H., Takano, T., Takahashi, T., Noda, T., & Okano, H. (2005). The RNA-binding protein HuD regulates neuronal cell identity and maturation. *Proceedings of the National Academy of Sciences of the United States of America*. https://doi.org/10.1073/pnas.0407523102

Åkerblom, M., Sachdeva, R., Barde, I., Verp, S., Gentner, B., Trono, D., & Jakobsson, J. (2012). MicroRNA-124 is a subventricular zone neuronal fate determinant. *Journal of Neuroscience*. https://doi.org/10.1523/JNEUROSCI.0558-12.2012

Ambasudhan, R., Talantova, M., Coleman, R., Yuan, X., Zhu, S., Lipton, S. A., & Ding, S. (2011). Direct reprogramming of adult human fibroblasts to functional neurons under defined conditions. *Cell Stem Cell*. https://doi.org/10.1016/j.stem.2011.07.002

Aravantinou-Fatorou, K., Ortega, F., Chroni-Tzartou, D., Antoniou, N., Poulopoulou, C., Politis, P. K., Berninger, B., Matsas, R., & Thomaidou, D. (2015). CEND1 and NEUROGENIN2 Reprogram Mouse Astrocytes and Embryonic Fibroblasts to Induced Neural Precursors and Differentiated Neurons. *Stem Cell Reports*, *5*(3), 405–418. https://doi.org/10.1016/j.stemcr.2015.07.012

Baudet, M. L., Zivraj, K. H., Abreu-Goodger, C., Muldal, A., Armisen, J., Blenkiron, C., Goldstein, L. D., Miska, E. A., & Holt, C. E. (2012). MiR-124 acts through CoREST to control onset of Sema3A sensitivity in navigating retinal growth cones. *Nature Neuroscience*. https://doi.org/10.1038/nn.2979

Berninger, B., Costa, M. R., Koch, U., Schroeder, T., Sutor, B., Grothe, B., & Götz, M. (2007). Functional properties of neurons derived from in vitro reprogrammed postnatal astroglia. *Journal of Neuroscience*. https://doi.org/10.1523/JNEUROSCI.1615-07.2007

Birtele, M., Sharma, Y., Kidnapillai, S., Lau, S., Stoker, T. B., Barker, R. A., Rylander Ottosson, D., Drouin-Ouellet, J., & Parmar, M. (2019). Dual modulation of neuron-specific microRNAs and the REST complex promotes functional maturation of human adult induced neurons. *FEBS Letters*. https://doi.org/10.1002/1873-3468.13612

Boudreau, R. L., Jiang, P., Gilmore, B. L., Spengler, R. M., Tirabassi, R., Nelson, J. A., Ross, C. A., Xing, Y., & Davidson, B. L. (2014). Transcriptome-wide discovery of microRNA binding sites in Human Brain. *Neuron*. https://doi.org/10.1016/j.neuron.2013.10.062

Bray, N. L., Pimentel, H., Melsted, P., & Pachter, L. (2016). Near-optimal probabilistic RNA-seq quantification. *Nature Biotechnology*. https://doi.org/10.1038/nbt.3519

Carrick, D. M., & Blackshear, P. J. (2007). Comparative expression of tristetraprolin (TTP) family member transcripts in normal human tissues and cancer cell lines. *Archives of Biochemistry and Biophysics*. https://doi.org/10.1016/j.abb.2007.04.011

Chen, M. T., Dong, L., Zhang, X. H., Yin, X. L., Ning, H. M., Shen, C., Su, R., Li, F., Song, L., Ma, Y. N., Wang, F., Zhao, H. L., Yu, J., & Zhang, J. W. (2015). ZFP36L1 promotes monocyte/macrophage differentiation by repressing CDK6. *Scientific Reports*. https://doi.org/10.1038/srep16229

Cheng, L. C., Pastrana, E., Tavazoie, M., & Doetsch, F. (2009). MiR-124 regulates adult neurogenesis in the subventricular zone stem cell niche. *Nature Neuroscience*. https://doi.org/10.1038/nn.2294

Chi, S. W., Zang, J. B., Mele, A., & Darnell, R. B. (2009). Argonaute HITS-CLIP decodes microRNA-mRNA interaction maps. *Nature*. https://doi.org/10.1038/nature08170

Cunningham, F., Achuthan, P., Akanni, W., Allen, J., Amode, M. R., Armean, I. M., Bennett, R., Bhai, J., Billis, K., Boddu, S., Cummins, C., Davidson, C., Dodiya, K. J., Gall, A., Girón, C. G., Gil, L., Grego, T., Haggerty, L., Haskell, E., … Flicek, P. (2019). Ensembl 2019. *Nucleic Acids Research*. https://doi.org/10.1093/nar/gky1113

Dai, W., Li, W., Hoque, M., Li, Z., Tian, B., & Makeyev, E. V. (2015). A post-transcriptional mechanism pacing expression of neural genes with precursor cell differentiation status. *Nature*

Communications. https://doi.org/10.1038/ncomms8576

Davis, M. P. A., van Dongen, S., Abreu-Goodger, C., Bartonicek, N., & Enright, A. J. (2013). Kraken: A set of tools for quality control and analysis of high-throughput sequence data. *Methods*. https://doi.org/10.1016/j.ymeth.2013.06.027

DeBoer, E. M., Kraushar, M. L., Hart, R. P., & Rasin, M. R. (2013). Post-transcriptional regulatory elements and spatiotemporal specification of neocortical stem cells and projection neurons. In *Neuroscience*. https://doi.org/10.1016/j.neuroscience.2013.05.042

Deo, M., Yu, J. Y., Chung, K. H., Tippens, M., & Turner, D. L. (2006). Detection of mammalian microRNA expression by in situ hybridization with RNA oligonucleotides. *Developmental Dynamics*. https://doi.org/10.1002/dvdy.20847

Díaz-Guerra, E., Pignatelli, J., Nieto-Estévez, V., & Vicario-Abejón, C. (2013). Transcriptional regulation of olfactory bulb neurogenesis. *Anatomical Record*. https://doi.org/10.1002/ar.22733

Dioum, E. M., Osborne, J. K., Goetsch, S., Russell, J., Schneider, J. W., & Cobb, M. H. (2011). A small molecule differentiation inducer increases insulin production by pancreatic β cells. *Proceedings of the National Academy of Sciences of the United States of America*. https://doi.org/10.1073/pnas.1118526109

Elsen, G. E., Bedogni, F., Hodge, R. D., Bammler, T. K., MacDonald, J. W., Lindtner, S., Rubenstein, J. L. R., & Hevner, R. F. (2018). The epigenetic factor landscape of developing neocortex is regulated by transcription factors Pax6→ Tbr2→ Tbr1. *Frontiers in Neuroscience*. https://doi.org/10.3389/fnins.2018.00571

Gabel, S., Koncina, E., Dorban, G., Heurtaux, T., Birck, C., Glaab, E., Michelucci, A., Heuschling, P., & Grandbarbe, L. (2016). Inflammation Promotes a Conversion of Astrocytes into Neural Progenitor Cells via NF-κB Activation. *Molecular Neurobiology*. https://doi.org/10.1007/s12035-015-9428-3

Galloway, A., Saveliev, A., Łukasiak, S., Hodson, D. J., Bolland, D., Balmanno, K., Ahlfors, H., Monzón-Casanova, E., Mannurita, S. C., Bell, L. S., Andrews, S., Díaz-Muñoz, M. D., Cook, S. J., Corcoran, A., & Turner, M. (2016). RNA-binding proteins ZFP36L1 and ZFP36L2 promote cell quiescence. *Science*. https://doi.org/10.1126/science.aad5978

Gao, L., Guan, W., Wang, M., Wang, H., Yu, J., Liu, Q., Qiu, B., Yu, Y., Ping, Y., Bian, X., Shen, L., & Pei, G. (2017). Direct Generation of Human Neuronal Cells from Adult Astrocytes by Small Molecules. *Stem Cell Reports*. https://doi.org/10.1016/j.stemcr.2017.01.014

Gascón, S., Murenu, E., Masserdotti, G., Ortega, F., Russo, G. L., Petrik, D., Deshpande, A., Heinrich, C., Karow, M., Robertson, S. P., Schroeder, T., Beckers, J., Irmler, M., Berndt, C., Angeli, J. P. F., Conrad, M., Berninger, B., & Götz, M. (2016). Identification and Successful Negotiation of a Metabolic Checkpoint in Direct Neuronal Reprogramming. *Cell Stem Cell*, *18*(3), 396–409. https://doi.org/10.1016/j.stem.2015.12.003

Götz, M., Sirko, S., Beckers, J., & Irmler, M. (2015). Reactive astrocytes as neural stem or progenitor cells: In vivo lineage, In vitro potential, and Genome-wide expression analysis. In *GLIA*. https://doi.org/10.1002/glia.22850

Grande, A., Sumiyoshi, K., López-Juárez, A., Howard, J., Sakthivel, B., Aronow, B., Campbell, K., & Nakafuku, M. (2013). Environmental impact on direct neuronal reprogramming in vivo in the adult brain. *Nature Communications*, *4*. https://doi.org/10.1038/ncomms3373

Gross, R. E., Mehler, M. F., Mabie, P. C., Zang, Z., Santschi, L., & Kessler, J. A. (1996). Bone morphogenetic proteins promote astroglial lineage commitment by mammalian subventricular zone progenitor cells. *Neuron*. https://doi.org/10.1016/S0896-6273(00)80193-2

Guo, Z., Zhang, L., Wu, Z., Chen, Y., Wang, F., & Chen, G. (2014). In vivo direct reprogramming of reactive glial cells into functional neurons after brain injury and in an Alzheimer's disease model. *Cell Stem Cell*, *14*(2), 188–202. https://doi.org/10.1016/j.stem.2013.12.001

Heinrich, C., Blum, R., Gascón, S., Masserdotti, G., Tripathi, P., Sánchez, R., Tiedt, S., Schroeder, T., Götz, M., & Berninger, B. (2010). Directing astroglia from the cerebral cortex into subtype specific functional neurons. *PLoS Biology*. https://doi.org/10.1371/journal.pbio.1000373

Huh, C. J., Zhang, B., Victor, M. B., Dahiya, S., Batista, L. F. Z., Horvath, S., & Yoo, A. S. (2016). Maintenance of age in human neurons generated by microRNA-based neuronal conversion of fibroblasts. *ELife*. https://doi.org/10.7554/eLife.18648

Jiang, H., Xu, Z., Zhong, P., Ren, Y., Liang, G., Schilling, H. A., Hu, Z., Zhang, Y., Wang, X., Chen, S., Yan, Z., & Feng, J. (2015). Cell cycle and p53 gate the direct conversion of human fibroblasts to dopaminergic neurons. *Nature Communications*. https://doi.org/10.1038/ncomms10100

909 Kang, W., & Hébert, J. M. (2011). Signaling pathways in reactive astrocytes, a genetic perspective. In
910 *Molecular Neurobiology*. https://doi.org/10.1007/s12035-011-8163-7
911 Krueger, F. (2015). Trim Galore!: A wrapper tool around Cutadapt and FastQC to consistently apply
912 quality and adapter trimming to FastQ files. *Babraham Institute*.
913 Kwan, K. Y., Šestan, N., & Anton, E. S. (2012). Transcriptional co-regulation of neuronal migration and
914 laminar identity in the neocortex. In *Development*. https://doi.org/10.1242/dev.069963
915 Lai, W. S., Carballo, E., Thorn, J. M., Kennington, E. A., & Blackshear, P. J. (2000). Interactions of CCCH
916 zinc finger proteins with mRNA. Binding of tristetraprolin-related zinc finger proteins to AU-rich
917 elements and destabilization of mRNA. *Journal of Biological Chemistry*.
918 https://doi.org/10.1074/jbc.M001696200
919 Lee, S. W., Oh, Y. M., Lu, Y. L., Kim, W. K., & Yoo, A. S. (2018). MicroRNAs Overcome Cell Fate Barrier
920 by Reducing EZH2-Controlled REST Stability during Neuronal Conversion of Human Adult
921 Fibroblasts. *Developmental Cell*. https://doi.org/10.1016/j.devcel.2018.06.007
922 Li, Xiang, Zuo, X., Jing, J., Ma, Y., Wang, J. J., Liu, D., Zhu, J., Du, X., Xiong, L., Du, Y., Xu, J., Xiao, X.,
923 Wang, J. J., Chai, Z., Zhao, Y., & Deng, H. (2015). Small-Molecule-Driven Direct Reprogramming
924 of Mouse Fibroblasts into Functional Neurons. *Cell Stem Cell*, *17*(2), 195–203.
925 https://doi.org/10.1016/j.stem.2015.06.003
926 Li, Xuekun, & Jin, P. (2010). Roles of small regulatory RNAs in determining neuronal identity. In *Nature*
927 *Reviews Neuroscience*. https://doi.org/10.1038/nrn2739
928 Lim, R. G., Salazar, L. L., Wilton, D. K., King, A. R., Stocksdale, J. T., Sharifabad, D., Lau, A. L., Stevens,
929 B., Reidling, J. C., Winokur, S. T., Casale, M. S., Thompson, L. M., Pardo, M., Díaz-Barriga, A. G.
930 G., Straccia, M., Sanders, P., Alberch, J., Canals, J. M., Kaye, J. A., … Svendsen, C. N. (2017).
931 Developmental alterations in Huntington's disease neural cells and pharmacological rescue in
932 cells and mice. *Nature Neuroscience*, *20*(5), 648–660. https://doi.org/10.1038/nn.4532
933 Liu, K., Liu, Y., Mo, W., Qiu, R., Wang, X., Wu, J. Y., & He, R. (2011). MiR-124 regulates early
934 neurogenesis in the optic vesicle and forebrain, targeting NeuroD1. *Nucleic Acids Research*.
935 https://doi.org/10.1093/nar/gkq904
936 Luján, R., Shigemoto, R., & López-Bendito, G. (2005). Glutamate and GABA receptor signalling in the
937 developing brain. In *Neuroscience*. https://doi.org/10.1016/j.neuroscience.2004.09.042
938 Magnusson, J. P., Göritz, C., Tatarishvili, J., Dias, D. O., Smith, E. M. K., Lindvall, O., Kokaia, Z., & Frisén,
939 J. (2014). A latent neurogenic program in astrocytes regulated by Notch signaling in the mouse.
940 *Science*. https://doi.org/10.1126/science.346.6206.237
941 Maiorano, N. A., & Mallamaci, A. (2009). Promotion of embryonic cortico-cerebral neuronogenesis by
942 miR-124. *Neural Development*. https://doi.org/10.1186/1749-8104-4-40
943 Makeyev, E. V., Zhang, J., Carrasco, M. A., & Maniatis, T. (2007). The MicroRNA miR-124 Promotes
944 Neuronal Differentiation by Triggering Brain-Specific Alternative Pre-mRNA Splicing. *Molecular*
945 *Cell*. https://doi.org/10.1016/j.molcel.2007.07.015
946 Martin, M. (2011). Cutadapt removes adapter sequences from high-throughput sequencing reads.
947 *EMBnet.Journal*. https://doi.org/10.14806/ej.17.1.200
948 Matsuda, T., Irie, T., Katsurabayashi, S., Hayashi, Y., Nagai, T., Hamazaki, N., Adefuin, A. M. D., Miura,
949 F., Ito, T., Kimura, H., Shirahige, K., Takeda, T., Iwasaki, K., Imamura, T., & Nakashima, K. (2019).
950 Pioneer Factor NeuroD1 Rearranges Transcriptional and Epigenetic Profiles to Execute
951 Microglia-Neuron Conversion. *Neuron*. https://doi.org/10.1016/j.neuron.2018.12.010
952 Mattugini, N., Bocchi, R., Scheuss, V., Russo, G. L., Torper, O., Lao, C. L., & Götz, M. (2019). Inducing
953 Different Neuronal Subtypes from Astrocytes in the Injured Mouse Cerebral Cortex. *Neuron*,
954 *103*(6), 1086-1095.e5. https://doi.org/10.1016/j.neuron.2019.08.009
955 Neo, W. H., Yap, K., Lee, S. H., Looi, L. S., Khandelia, P., Neo, S. X., Makeyev, E. V., & Su, I. H. (2014).
956 MicroRNA miR-124 controls the choice between neuronal and astrocyte differentiation by fine-
957 tuning Ezh2 expression. *Journal of Biological Chemistry*.
958 https://doi.org/10.1074/jbc.M113.525493
959 Niu, W., Zang, T., Zou, Y., Fang, S., Smith, D. K., Bachoo, R., & Zhang, C. L. (2013). In vivo
960 reprogramming of astrocytes to neuroblasts in the adult brain. *Nature Cell Biology*, *15*(10),
961 1164–1175. https://doi.org/10.1038/ncb2843
962 Paraskevopoulou, M. D., Karagkouni, D., Vlachos, I. S., Tastsoglou, S., & Hatzigeorgiou, A. G. (2018).
963 microCLIP super learning framework uncovers functional transcriptome-wide miRNA
964 interactions. *Nature Communications*. https://doi.org/10.1038/s41467-018-06046-y
965 Pascale, A., Amadio, M., & Quattrone, A. (2008). Defining a neuron: Neuronal ELAV proteins. In

Cellular and Molecular Life Sciences. https://doi.org/10.1007/s00018-007-7017-y

Pataskar, A., Jung, J., Smialowski, P., Noack, F., Calegari, F., Straub, T., & Tiwari, V. K. (2016). NeuroD1 reprograms chromatin and transcription factor landscapes to induce the neuronal program. *The EMBO Journal*. https://doi.org/10.15252/embj.201591206

Pimentel, H., Bray, N. L., Puente, S., Melsted, P., & Pachter, L. (2017). Differential analysis of RNA-seq incorporating quantification uncertainty. *Nature Methods*. https://doi.org/10.1038/nmeth.4324

Rivetti Di Val Cervo, P., Romanov, R. A., Spigolon, G., Masini, D., Martín-Montañez, E., Toledo, E. M., La Manno, G., Feyder, M., Pifl, C., Ng, Y. H., Sánchez, S. P., Linnarsson, S., Wernig, M., Harkany, T., Fisone, G., & Arenas, E. (2017). Induction of functional dopamine neurons from human astrocytes in vitro and mouse astrocytes in a Parkinson's disease model. *Nature Biotechnology*. https://doi.org/10.1038/nbt.3835

Sanuki, R., Onishi, A., Koike, C., Muramatsu, R., Watanabe, S., Muranishi, Y., Irie, S., Uneo, S., Koyasu, T., Matsui, R., Chérasse, Y., Urade, Y., Watanabe, D., Kondo, M., Yamashita, T., & Furukawa, T. (2011). MiR-124a is required for hippocampal axogenesis and retinal cone survival through Lhx2 suppression. *Nature Neuroscience*. https://doi.org/10.1038/nn.2897

Scheckel, C., Drapeau, E., Frias, M. A., Park, C. Y., Fak, J., Zucker-Scharff, I., Kou, Y., Haroutunian, V., Ma'ayan, A., Buxbaum, J. D., & Darnell, R. B. (2016). Regulatory consequences of neuronal ELAV-like protein binding to coding and non-coding RNAs in human brain. *ELife*. https://doi.org/10.7554/eLife.10421

Schneider, J. W., Gao, Z., Li, S., Farooqi, M., Tang, T. S., Bezprozvanny, I., Frantz, D. E., & Hsieh, J. (2008). Small-molecule activation of neuronal cell fate. *Nature Chemical Biology*, *4*(7), 408–410. https://doi.org/10.1038/nchembio.95

Sirko, S., Behrendt, G., Johansson, P. A., Tripathi, P., Costa, M., Bek, S., Heinrich, C., Tiedt, S., Colak, D., Dichgans, M., Fischer, I. R., Plesnila, N., Staufenbiel, M., Haass, C., Snapyan, M., Saghatelyan, A., Tsai, L. H., Fischer, A., Grobe, K., … Götz, M. (2013). Reactive glia in the injured brain acquire stem cell properties in response to sonic hedgehog glia. *Cell Stem Cell*. https://doi.org/10.1016/j.stem.2013.01.019

Tang, J., Yoo, A. S., & Crabtree, G. R. (2013a). Reprogramming human fibroblasts to neurons by recapitulating an essential microRNA-chromatin switch. In *Current Opinion in Genetics and Development*. https://doi.org/10.1016/j.gde.2013.07.001

Tang, J., Yoo, A. S., & Crabtree, G. R. (2013b). Reprogramming human fibroblasts to neurons by recapitulating an essential microRNA-chromatin switch. In *Current Opinion in Genetics and Development* (Vol. 23, Issue 5, pp. 591–598). https://doi.org/10.1016/j.gde.2013.07.001

Torper, O., Pfisterer, U., Wolf, D. A., Pereira, M., Lau, S., Jakobsson, J., Björklund, A., Grealish, S., & Parmar, M. (2013). Generation of induced neurons via direct conversion in vivo. *Proceedings of the National Academy of Sciences of the United States of America*, *110*(17), 7038–7043. https://doi.org/10.1073/pnas.1303829110

Victor, M. B., Richner, M., Hermanstyne, T. O., Ransdell, J. L., Sobieski, C., Deng, P. Y., Klyachko, V. A., Nerbonne, J. M., & Yoo, A. S. (2014). Generation of Human Striatal Neurons by MicroRNA-Dependent Direct Conversion of Fibroblasts. *Neuron*. https://doi.org/10.1016/j.neuron.2014.10.016

Victor, M. B., Richner, M., Olsen, H. E., Lee, S. W., Monteys, A. M., Ma, C., Huh, C. J., Zhang, B., Davidson, B. L., Yang, X. W., & Yoo, A. S. (2018). Striatal neurons directly converted from Huntington's disease patient fibroblasts recapitulate age-associated disease phenotypes. *Nature Neuroscience*. https://doi.org/10.1038/s41593-018-0075-7

Visvanathan, J., Lee, S. K. S., Lee, B., Lee, J. W., & Lee, S. K. S. (2007). The microRNA miR-124 antagonizes the anti-neural REST/SCP1 pathway during embryonic CNS development. *Genes and Development*. https://doi.org/10.1101/gad.1519107

Vogel, K. U., Bell, L. S., Galloway, A., Ahlfors, H., & Turner, M. (2016). The RNA-Binding Proteins Zfp36l1 and Zfp36l2 Enforce the Thymic β-Selection Checkpoint by Limiting DNA Damage Response Signaling and Cell Cycle Progression. *The Journal of Immunology*. https://doi.org/10.4049/jimmunol.1600854

Volvert, M. L., Prévot, P. P., Close, P., Laguesse, S., Pirotte, S., Hemphill, J., Rogister, F., Kruzy, N., Sacheli, R., Moonen, G., Deiters, A., Merkenschlager, M., Chariot, A., Malgrange, B., Godin, J. D., & Nguyen, L. (2014). MicroRNA targeting of CoREST controls polarization of migrating cortical neurons. *Cell Reports*. https://doi.org/10.1016/j.celrep.2014.03.075

Weng, Q., Wang, J., Wang, J., He, D., Cheng, Z., Zhang, F., Verma, R., Xu, L., Dong, X., Liao, Y., He, X.,

Potter, A., Zhang, L., Zhao, C., Xin, M., Zhou, Q., Aronow, B. J., Blackshear, P. J., Rich, J. N., … Lu, Q. R. (2019). Single-Cell Transcriptomics Uncovers Glial Progenitor Diversity and Cell Fate Determinants during Development and Gliomagenesis. *Cell Stem Cell*. https://doi.org/10.1016/j.stem.2019.03.006

Wohl, S. G., & Reh, T. A. (2016). miR-124-9-9* potentiates Ascl1-induced reprogramming of cultured Müller glia. *GLIA*. https://doi.org/10.1002/glia.22958

Wu, T. D., & Nacu, S. (2010). Fast and SNP-tolerant detection of complex variants and splicing in short reads. *Bioinformatics*. https://doi.org/10.1093/bioinformatics/btq057

Yang, C., Iyer, R. R., Yu, A. C. H., Yong, R. L., Park, D. M., Weil, R. J., Ikejiri, B., Brady, R. O., Lonser, R. R., & Zhuang, Z. (2012). β-catenin signaling initiates the activation of astrocytes and its dysregulation contributes to the pathogenesis of astrocytomas. *Proceedings of the National Academy of Sciences of the United States of America*. https://doi.org/10.1073/pnas.1118754109

Yeom, K. H., Mitchell, S., Linares, A. J., Zheng, S., Lin, C. H., Wang, X. J., Hoffmann, A., & Black, D. L. (2018). Polypyrimidine tract-binding protein blocks miRNA-124 biogenesis to enforce its neuronal-specific expression in the mouse. *Proceedings of the National Academy of Sciences of the United States of America*. https://doi.org/10.1073/pnas.1809609115

Yoo, A. S., Staahl, B. T., Chen, L., & Crabtree, G. R. (2009a). MicroRNA-mediated switching of chromatin-remodelling complexes in neural development. *Nature*. https://doi.org/10.1038/nature08139

Yoo, A. S., Staahl, B. T., Chen, L., & Crabtree, G. R. (2009b). MicroRNA-mediated switching of chromatin-remodelling complexes in neural development. *Nature*, *460*(7255), 642–646. https://doi.org/10.1038/nature08139

Yoo, A. S., Sun, A. X., Li, L., Shcheglovitov, A., Portmann, T., Li, Y., Lee-Messer, C., Dolmetsch, R. E., Tsien, R. W., & Crabtree, G. R. (2011). MicroRNA-mediated conversion of human fibroblasts to neurons. In *Nature*. https://doi.org/10.1038/nature10323

Yuzwa, S. A., Borrett, M. J., Innes, B. T., Voronova, A., Ketela, T., Kaplan, D. R., Bader, G. D., & Miller, F. D. (2017). Developmental Emergence of Adult Neural Stem Cells as Revealed by Single-Cell Transcriptional Profiling. *Cell Reports*. https://doi.org/10.1016/j.celrep.2017.12.017

Zhang, Lei, Yin, J. C., Yeh, H., Ma, N. X., Lee, G., Chen, X. A., Wang, Y., Lin, L., Chen, L., Jin, P., Wu, G. Y., & Chen, G. (2015). Small Molecules Efficiently Reprogram Human Astroglial Cells into Functional Neurons. *Cell Stem Cell*. https://doi.org/10.1016/j.stem.2015.09.012

Zhang, Ling, Li, P., Hsu, T., Aguilar, H. R., Frantz, D. E., Schneider, J. W., Bachoo, R. M., & Hsieh, J. (2011). Small-molecule blocks malignant astrocyte proliferation and induces neuronal gene expression. *Differentiation*. https://doi.org/10.1016/j.diff.2011.02.005

Zhang, Y., Chen, K., Sloan, S. A., Bennett, M. L., Scholze, A. R., O'Keeffe, S., Phatnani, H. P., Guarnieri, P., Caneda, C., Ruderisch, N., Deng, S., Liddelow, S. A., Zhang, C., Daneman, R., Maniatis, T., Barres, B. A., & Wu, J. Q. (2014). An RNA-sequencing transcriptome and splicing database of glia, neurons, and vascular cells of the cerebral cortex. *Journal of Neuroscience*. https://doi.org/10.1523/JNEUROSCI.1860-14.2014

Figure legends

Figure 1: miR-124 is potent to instruct reprogramming of postnatal cortical astrocytes to iNs

(A) Overview of the miR-124 reprogramming protocol. **(B)** Immunostaining of astrocytes reprogrammed with miR-124 at day7 and day14 of the reprogramming protocol with Tuj1. **(C)** Quantification of the percentage of Tuj1+ reprogrammed cells (average ± SD, n=4 independent experiments, **p<0,01 and ***p<0,001 versus sc-miRNA). RT-qPCR analysis of the mRNA levels of the proneural TFs, Mash1 and Neurog2 **(D)**, the dorsal telencephalon TFs, Tbr2, Tbr1, Fezf2, Cux1 **(E)**, the ventral telencephalon TFs, Gsx2 and Dlx1 **(F),** and the neuronal differentiation TFs, Sox4, Sox11, Hes6 and NeuroD1 **(G)**. Data are presented as fold change versus sc-miRNA (average ± SD, n=3 independent experiments, **p<0,01 and ***p<0,001 versus sc-miRNA). **(H)** Co-immunostaining of astrocytes reprogrammed with miR-124 at day7 of the reprogramming protocol with Mash1/Tuj1, Tbr2/Tuj1 and Gsx2/Tuj1 antibodies. **(I)** Quantification of the percentage of Mash1+, Tbr2+ and Gsx2+ in Tuj1+ reprogrammed cells (average ± SD, n=3 independent experiments, **p<0,01 and ***p<0,001 versus sc-miRNA).

Figure 2: The neurogenic compound ISX9 greatly improves the miR-124-induced reprogramming efficiency and differentiation state of iNs

(A) Immunostaining of astrocytes reprogrammed with miR-124 or miR-124 along with ISX9 at day7 and day14 of the reprogramming protocol with Tuj1. **(B)** Quantification of the percentage of Tuj1+ reprogrammed cells at the time points day1, day5, day7, day10 and day14 of the reprogramming protocol (average ± SD, n=3 independent experiments for day5 and day10, n=8 for day7 and n=4 for day14, *p<0,05 and ***p<0,001 versus miR-124). **(C)** RT-qPCR analysis of the mRNA levels of NeuroD1 at day7 of the reprogramming protocol. Data are presented as log_2(fold change) versus sc-miRNA (average ± SD, n=3 independent experiments, **p<0,01 and ***p<0,001 versus sc-miRNA). **(D)** RT-qPCR analysis of the mRNA levels of the TFs, Neurog2, Mash1 and Tbr2 at the time points day1, day5, day7, day10 and day14 of the reprogramming protocol. Data are presented as log_2(fold change) versus astrocytes (day1). **(E)** Co-immunostaining of astrocytes reprogrammed with miR-124 along with ISX9 at day7 of the reprogramming protocol with Mash1/Tuj1, Tbr2/Tuj1 and Gsx2/Tuj1 antibodies. **(F)** Quantification of the percentage of Mash1+, Tbr2+ and Gsx2+ in Tuj1+ reprogrammed cells (average ± SD, n=3 independent experiments, **p<0,01 versus miR-

124). Measurement of the mean nuclear fluorescence intensity of Tbr2 **(G)** and Mash1 **(H)** in Tuj1+ reprogrammed cells either with miR-124 or miR-124 along with ISX9 at day7 of the reprogramming protocol. A representative experiment is shown (n=326 cells for miR-124 and n=540 cells for miR-124+ISX9) of n=3 independent experiments (mean ± SD, ***p<0,001 versus miR-124).

Figure 3: miR-124+ISX9-iNs exhibit characteristics of mature, electrophysiologically active neurons

(A) Co-immunostaining of miR-124+ISX9-iNs at day21 of the reprogramming protocol with MAP2/Tuj1 and MAP2/Synapsin1 (Syn1) antibodies. **(B)** Quantification of the percentage of Tuj1+ miR-124-iNs and miR-124+ISX9-iNs at day21 of the reprogramming protocol. The percentage of MAP2/Syn1 double positive (DP) Tuj1+ iNs is shown in blue (average ± SD, n=3 independent experiments, ***p<0,001 refers to %MAP2/Syn1 DP in Tuj1+ miR-124+ISX9-iNs versus miR-124-iNs and $^{###}$p<0,001 refers to %Tuj1 miR-124+ISX9-iNs versus miR-124-iNs). **(C)** Micrograph of a representative iN analyzed in the electrophysiological study. **(D)** Superimposed traces of inward Na^+ currents and outward K^+ currents evoked by depolarizing voltage steps obtained from a miR-124+ISX9-iN (day22) (left panel). Superimposed traces of inward and outward currents evoked by the same protocol after 1 min pre-application of 1 µM TTX + 10 mM TEA, showing the inhibition of both inward and outward currents (middle panel), followed by full recovery of the current traces after 3 min wash of the cell (right panel). **(E)** Superimposed traces of inward Na^+ currents and outward K^+ currents evoked by depolarizing voltage steps obtained from a miR-124-iN (day27) (left panel) and a miR-124+ISX9-iN (day27) (right panel). **(F)** Example of a repetitive action potential induced from a mature miR-124+ISX9-iN (day27) by different current steps (injections) at the current clamp mode (the protocol of current clamp is shown upper right). Representative traces of ionic currents induced by application of the neurotransmitter GABA in two different concentrations (300 µM and 1 mM) obtained from a miR-124+ISX9-iN in the early stage of neuronal maturation (day22) **(G)** and the neurotransmitter glutamate in two different concentrations (100 µM and 300 µM) obtained from a miR-124+ISX9-iN in the late stage of maturation (day27) **(H)**. The cell membrane potential was held at -70 mV and the time of agonist application is indicated in bars above the traces. **(I)** Example of a mature miR-124+ISX9-iN (day27) that exhibits spontaneous electrical activity measured at -70mV.

Figure 4: RNA-seq analysis revealed unique and convergent molecular contributions of miR-124 and ISX9 in the reprogramming process

(A) Heat map analysis of 300 up- and down-regulated DEGs that belong to the GO terms: Glial cell differentiation, Gliogenesis, Astrocyte development, Generation of neurons, Neuron differentiation, Regulation of neuron differentiation, Neurotransmitter transport and Synaptic signaling. **(B)** GO analysis of biological processes for the up-regulated DEGs in miR-124-iNs vs astro (in orange) and miR-124+ISX9-iNs vs astro (in red). **(C)** GO analysis of biological processes for the down-regulated DEGs in miR-124-iNs vs astro. GO terms are ranked according to $\log_{10}$FDR and the intensity legends indicate the fold enrichment of each GO term. **(D)** Heat map analysis of 54 up-regulated differentially expressed TFs clustered according to the brain region they are developmentally expressed (telencephalon, retina, midbrain and hindbrain). The master regulatory TFs Mash1, Neurog2, NeuroD1 and Gli1 are also shown at the top of the heat map. RT-qPCR validation of the mRNA levels of the TFs (Scrt1 and Lhx6) and the epigenetic factor (EF) Chd5 that are expressed in telencephalon **(E)**, the TFs (En1, Foxa1 and Lmx1b) expressed in midbrain **(F)** and the TFs (Phox2a, Hoxc4) expressed in hindbrain **(G)** at day7 of the reprogramming protocol, (average ± SD, n=3 independent experiments, *p<0,05, **p<0,01, ***p<0,001 versus sc-miRNA). Data are presented as $\log_{10}$(fold change) **(E, G)** and $\log_2$(fold change) **(F)** versus sc-miRNA.

Figure 5: The RNA-binding protein Zfp36l1 is a novel direct target of miR-124 with a key role in miR-124-induced cell fate switch

(A) Venn diagram of the miR-124 targets, derived from AGO-HITS-CLIP and the RNA-Seq analysis. miR-124 targets were combined with a list of genes, expressed in astrocytes, resulting in a set of 130 genes. **(B)** miR-124 direct binding to the 3' UTR of Zfp36l1 and ZFP36L1, in mouse and human species respectively. miR-124 binds with perfect seed complementarity (7mer-M8 site) in both species. **(C)** RT-qPCR validation of the mRNA levels of miR-124 direct target Zfp36l1 (average ± SD, n=3 independent experiments, **p<0,01 and ***p<0,001 vs sc-miRNA). **(D)** GO analysis of biological processes for Zfp36l1 direct targets that are also significantly up-regulated in miR-124-iNs vs sc-miRNA astro RNA-Seq analysis. GO terms are ranked according to $\log_{10}$FDR and the intensity legend shows the fold enrichment of each GO term. **(E)** Volcano plot comparing the $\log_2$(fold change) of TPM values in the miR-124-iNs vs sc-miRNA astro condition versus the $\log_{10}$(FDR) values. Significantly up-regulated ($\log_2$(fold change)≥1, FDR<0,01) and down-regulated ($\log_2$(fold change)≤-1, FDR≤0,01) genes are shown in orange and green respectively. Labels of Zfp36l1

and neuronal-specific up-regulated genes that are also Zfp36l1 direct targets are portrayed. RT-qPCR validation of the mRNA levels of the neuronal RBPs that are Zfp36l1 targets (Elavl4 and Nova1) **(F)** and the other two members of the nElavl family (Elavl2 and Elavl3) **(G)**. Data are presented as log_2(fold change) versus sc-miRNA (average ± SD, n=3 independent experiments, *p<0,05, **p<0,01 and ***p<0,001 versus sc-miRNA).

Figure 6: Overexpression of mIR-124 with or without co-treatment with ISX9 leads to glial cell trans-differentiation towards a deep cortical layer neuronal fate *in vivo*

(A) Experimental Setup. **(B)** LV-124-transduced cells in the peritraumatic cortical parenchyma expressing the mature neuronal marker NeuN, 3 weeks after viral transduction. Inset area indicated in white frame. Scale bar 50µm. **(C)** Percentage of control LV-GFP and LV-124 transduced cells expressing the mature neuronal marker NeuN, 6 days and 3 weeks post-transduction with or without treatment with ISX9. LV-GFP 6 days vs. 3 weeks: p=0,104, LV-124 6 days vs. 3 weeks: p**=0,00116, LV-124 6 days vs. LV-124-ISX9 3 weeks: p**=0,00104, LV-GFP 3 weeks vs. LV-124 3 weeks: p**=0,0036, LV-GFP 3 weeks vs. LV-124-ISX9 3 weeks: p**=0,00337, LV-124 3 weeks vs. LV-124-ISX9 3 weeks: p=0,8427. n=4 for all groups and time points. **(D)** LV-miR-124-transduced cells in the peritraumatic cortical parenchyma expressing the deep layer cortical neuronal marker Tbr1 3 weeks after viral transduction. Image from an animal transduced with LV-miR-124 and co-treated with ISX9. Inset area indicated in white frame. White arrows indicate NeuN+/Tbr1+ transduced cells. Scale bar 50µm. **(E)** Percentage of LV-124-transduced cells expressing Tbr1, 3 weeks post-transduction with or without treatment with ISX9. LV-124 3 weeks vs. LV-124-ISX9 3 weeks: p=0,1503. n=4 for both groups.

Supplementary Figure 1 (related to Figure 2):

(A) Immunostaining of astrocytes transfected with sc-miRNA supplemented with ISX9 at day7 and day14 of the reprogramming protocol with Tuj1. **(B)** RT-qPCR analysis of the mRNA levels of Gsx2, Cux2, Fezf2 and Sox11 at day7 of the reprogramming protocol. Data are presented as log_2(fold change) versus sc-miRNA (average ± SD, n=3 independent experiments, *p<0,05, **p<0,01 and ***p<0,001 versus sc-miRNA). Measurement of the mean nuclear fluorescence intensity of Tbr2 **(C)** and Mash1 **(D)** in astrocytes trasfected either with sc-miRNA or miR-124 in the presence or absence of ISX9 at day7 of the reprogramming protocol. A representative experiment is shown of n=3 independent

1193 experiments (mean ± SD, n=250 cells for sc-miRNA, n=220 cells for sc-miRNA+ISX9, n=490 for
1194 miR-124 and n=450 cells for miR-124+ISX9).
1195
1196 **Supplementary Figure 2 (related to Figure 3):**

1197 **(A)** Co-immunostaining of miR124-iNs and miR-124+ISX9-iNs at day14 of the reprogramming
1198 protocol with Tbr1/Tuj1 antibodies. **(B)** Quantification of the percentage of Tuj1+ iNs at
1199 day14 of the reprogramming protocol. The percentage of Tbr1+/ Tuj1+ iNs is shown in blue
1200 (average ± SD, n=3 independent experiments, *p<0,05 refers to %Tuj1+ miR-124+ISX9-iNs
1201 versus miR-124-iNs, no statistical significant difference was found for %Tbr1+/Tuj1+ miR-
1202 124+ISX9-iNs versus miR-124-iNs). **(C)** A typical I-V curve from a mature miR-124+ISX9-iN
1203 (day27) under control conditions. Blue triangles show the V–I relationship for the potassium
1204 ion and red squares for the sodium ion, which is not linear, indicating that the sodium ion
1205 channel is voltage-dependent. Black circles indicate the I–V relationship derived from
1206 summing the sodium and potassium currents. **(D)** Superimposed traces obtained from a
1207 mature miR-124+ISX9-iN (day 26) with application of 100 µM glutamate or co-application of
1208 100 µM Glut + CNQX indicated that the antagonist CNQX inhibits the AMPA/
1209 kainate glutamate receptor.
1210
1211 **Supplementary Figure 3 (related to Figure 4):**

1212 **(A)** Heat map analysis of 35 down-regulated astrocytic TFs. **(B)** RT-qPCR validation of the
1213 mRNA levels of the TFs (Nfic, Tcf7l1, Rbpj, Tcf4) and the RBP Zfp36 expressed in astrocytes.
1214 Data are presented as fold change versus sc-miRNA (average ± SD, n=3 independent
1215 experiments, **p<0,01 and ***p<0,001 versus sc-miRNA). **(C)** Heat map analysis of 40 up-
1216 and down-regulated RBPs. **(D)** Heat map analysis of 22 up- and down-regulated epigenetic
1217 factors (EFs).
1218
1219 **Supplementary Figure 4 (related to figure 6):**

1220 **(A)** Image of astrogliosis (red, GFAP staining) on cortical trauma (white continuous line), 6
1221 days after stereotaxic injection of LV-124-GFP (transduced cells in green). CX: cortex. Scale
1222 bar: 100µm. **(B)** Brain cell types transduced by LV-GFP and LV-124. 6 days after
1223 transduction, LV-GFP and LV-124-GFP preferably transduce GFAP+ astrocytes, and to a
1224 lesser extent NeuN+ neurons, Olig2+ oligodendrocytes, and Iba-1+ microglia. LV-GFP vs. LV-
1225 124, for GFAP: p= 0,650, NeuN: p=0,209, Olig2: p=0,775, Iba-1: p=0,612. GFAP LV-GFP n=4,

1226 GFAP LV-124 n=4, NeuN LV-GFP n=4, NeuN LV-124 n=4, Olig2 LV-GFP n=4, Olig2 LV-124 n=3,

1227 Iba-1 LV-GFP n=4, Iba-1 LV-124. For all groups n=4.

1228

Figure 1

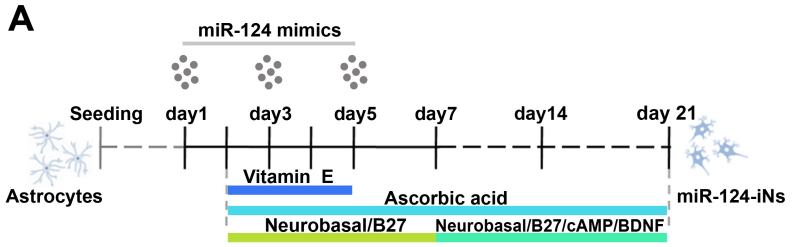
A
miR-124 mimics
Seeding
day1
day3
day5
day7
day14
day 21
Astrocytes
Vitamin E
Ascorbic acid
miR-124-iNs
Neurobasal/B27
Neurobasal/B27/cAMP/BDNF

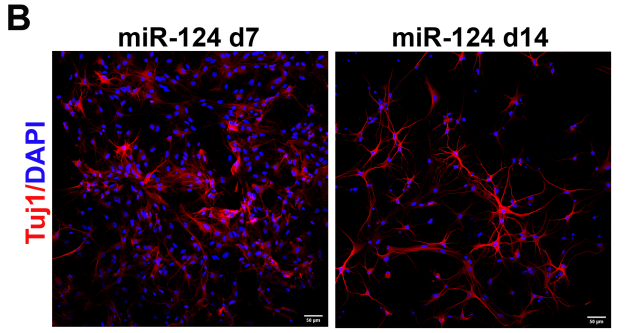
B
miR-124 d7
miR-124 d14
Tuj1/DAPI

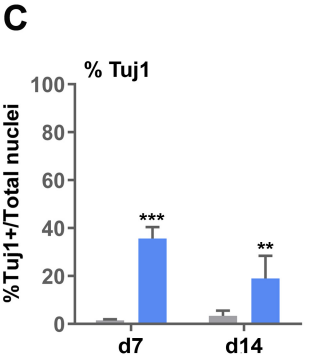
C
% Tuj1
%Tuj1+/Total nuclei
d7
d14

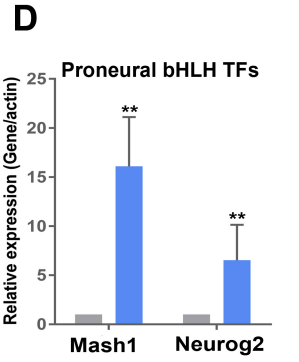
D
Proneural bHLH TFs
Relative expression (Gene/actin)
Mash1
Neurog2

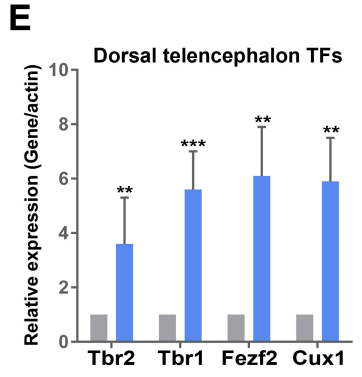
E
Dorsal telencephalon TFs
Relative expression (Gene/actin)
Tbr2
Tbr1
Fezf2
Cux1

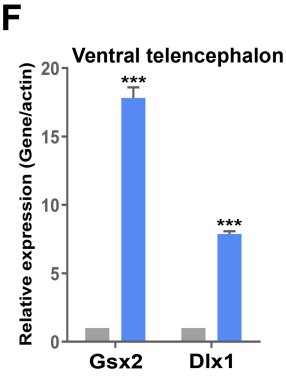
F
Ventral telencephalon TF
Relative expression (Gene/actin)
Gsx2
Dlx1

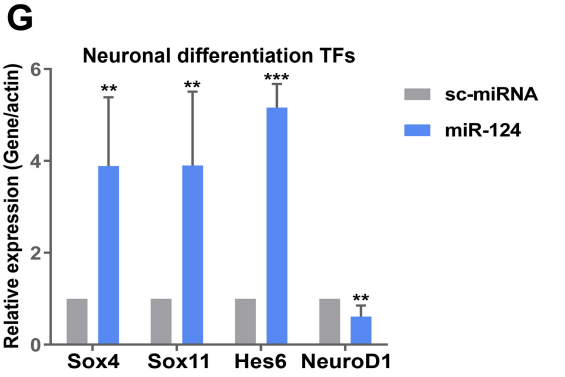
G
Neuronal differentiation TFs
Relative expression (Gene/actin)
Sox4
Sox11
Hes6
NeuroD1
sc-miRNA
miR-124

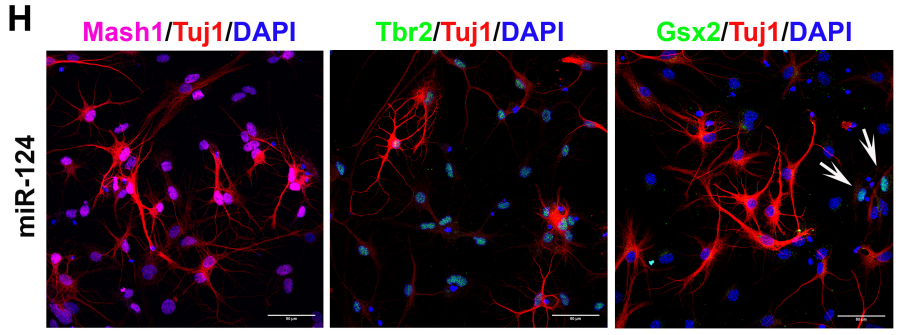
H
Mash1/Tuj1/DAPI
Tbr2/Tuj1/DAPI
Gsx2/Tuj1/DAPI
miR-124

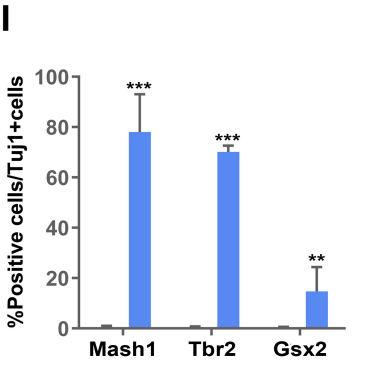
I
%Positive cells/Tuj1+cells
Mash1
Tbr2
Gsx2

Figure 2

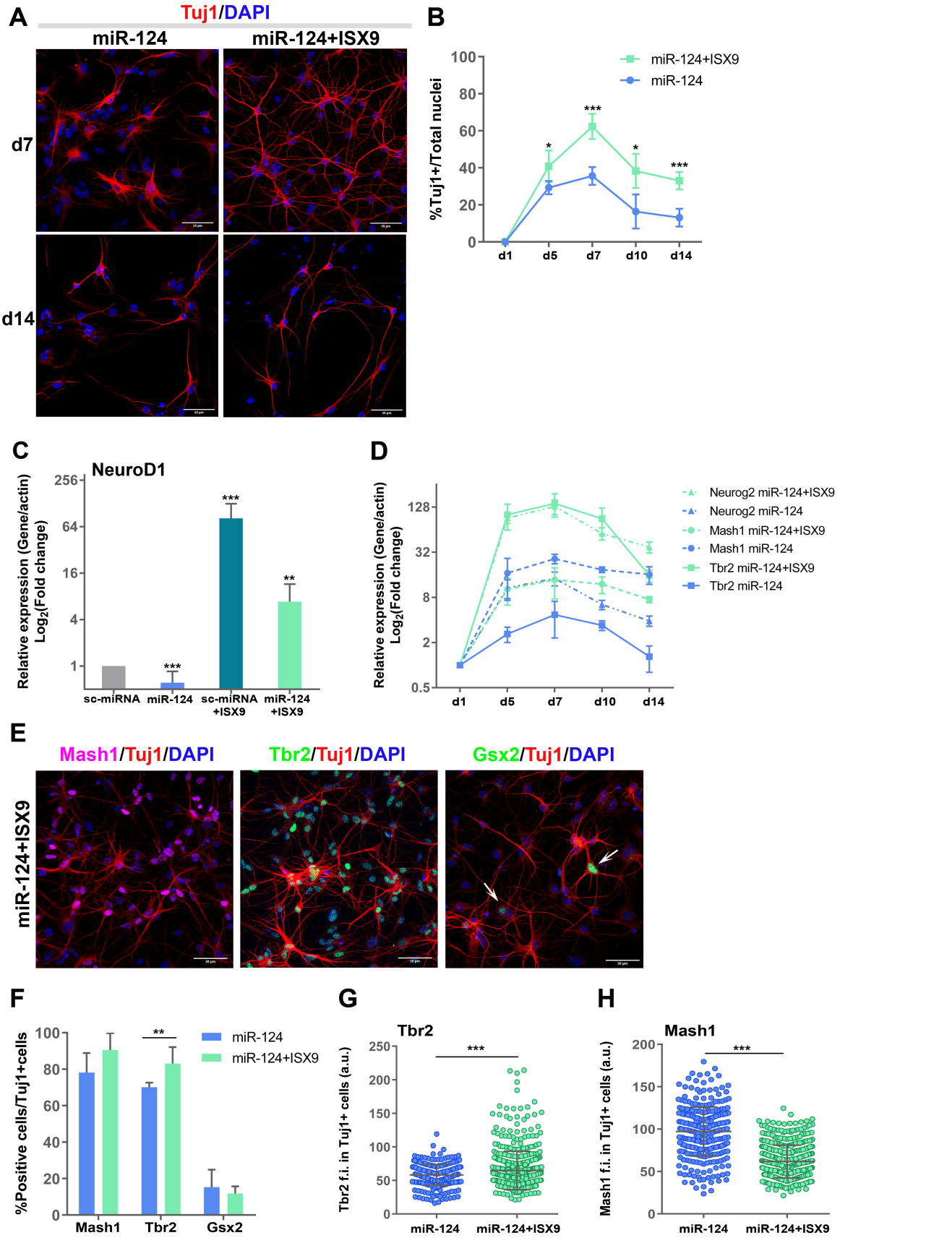
A
Tuj1/DAPI
miR-124
miR-124+ISX9
d7
d14
B
miR-124+ISX9
miR-124
%Tuj1+/Total nuclei
d1
d5
d7
d10
d14
C
NeuroD1
Relative expression (Gene/actin)
Log2(Fold change)
sc-miRNA
miR-124
sc-miRNA +ISX9
miR-124 +ISX9
D
Relative expression (Gene/actin)
Log2(Fold change)
Neurog2 miR-124+ISX9
Neurog2 miR-124
Mash1 miR-124+ISX9
Mash1 miR-124
Tbr2 miR-124+ISX9
Tbr2 miR-124
E
Mash1/Tuj1/DAPI
Tbr2/Tuj1/DAPI
Gsx2/Tuj1/DAPI
miR-124+ISX9
F
%Positive cells/Tuj1+cells
miR-124
miR-124+ISX9
Mash1
Tbr2
Gsx2
G
Tbr2
Tbr2 f.i. in Tuj1+ cells (a.u.)
miR-124
miR-124+ISX9
H
Mash1
Mash1 f.i. in Tuj1+ cells (a.u.)
miR-124
miR-124+ISX9

Figure 3

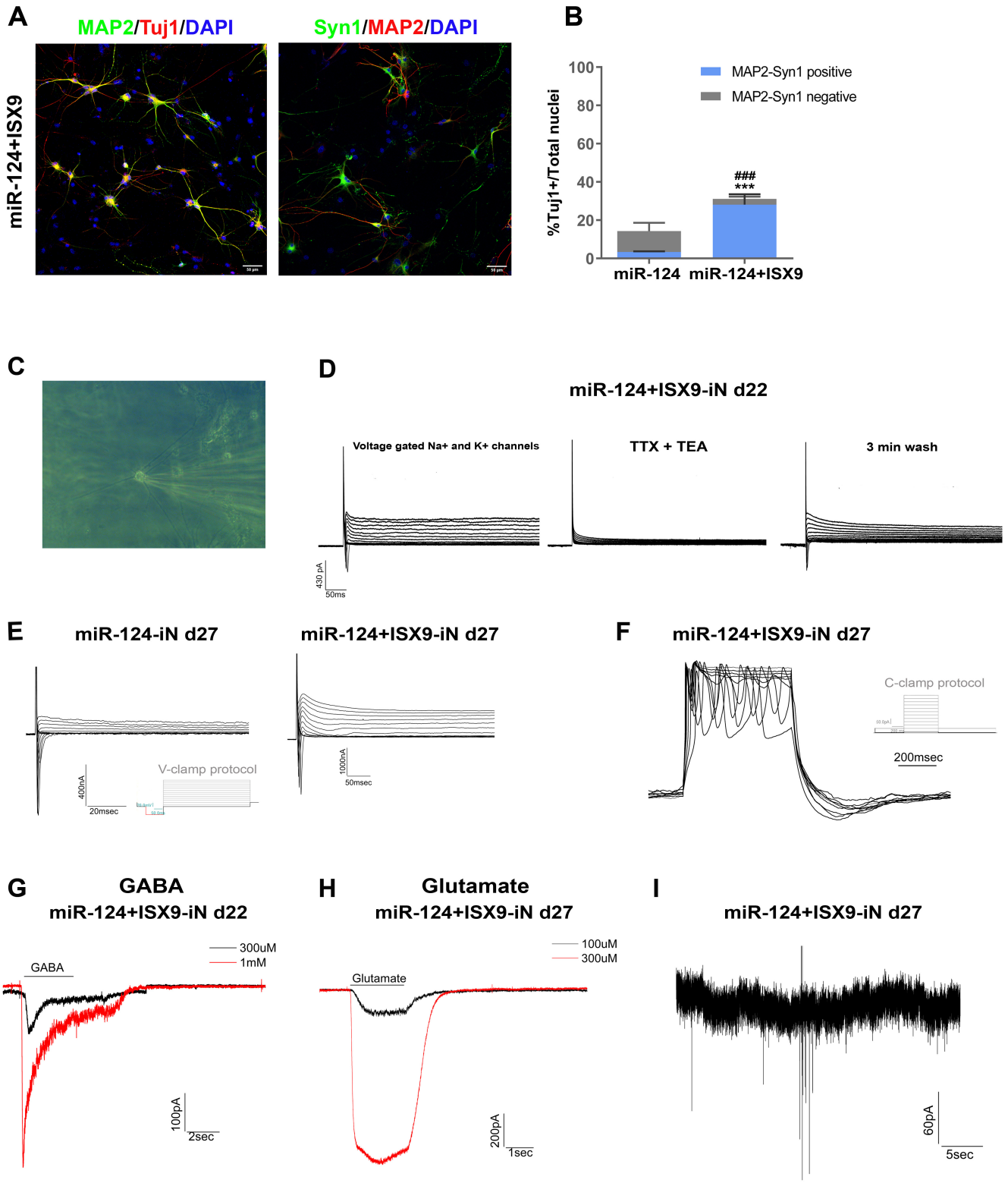
A
MAP2/Tuj1/DAPI
Syn1/MAP2/DAPI
miR-124+ISX9
B
MAP2-Syn1 positive
MAP2-Syn1 negative
%Tuj1+/Total nuclei
100
80
60
40
20
0
###
***
miR-124
miR-124+ISX9
C
D
miR-124+ISX9-iN d22
Voltage gated Na+ and K+ channels
TTX + TEA
3 min wash
430 pA
50ms
E
miR-124-iN d27
miR-124+ISX9-iN d27
400nA
20msec
V-clamp protocol
1000nA
50msec
F
miR-124+ISX9-iN d27
C-clamp protocol
200msec
G
GABA
miR-124+ISX9-iN d22
GABA
300uM
1mM
100pA
2sec
H
Glutamate
miR-124+ISX9-iN d27
Glutamate
100uM
300uM
200pA
1sec
I
miR-124+ISX9-iN d27
60pA
5sec

Figure 4

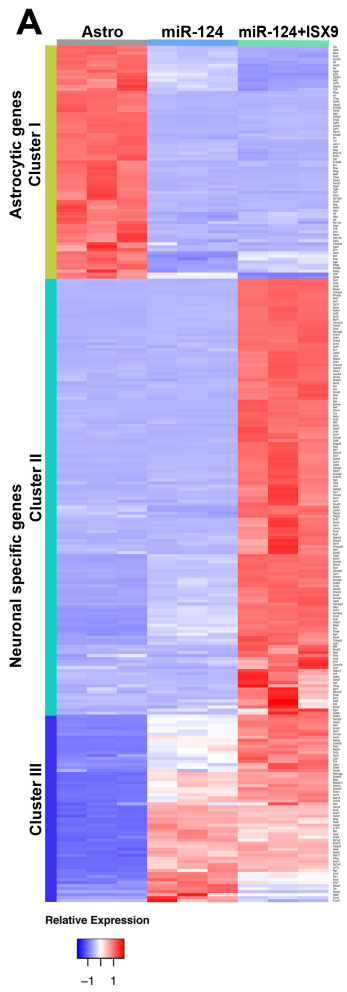
A
Astro
miR-124
miR-124+ISX9
Astrocytic genes
Cluster I
Neuronal specific genes
Cluster II
Cluster III
Relative Expression
−1
1

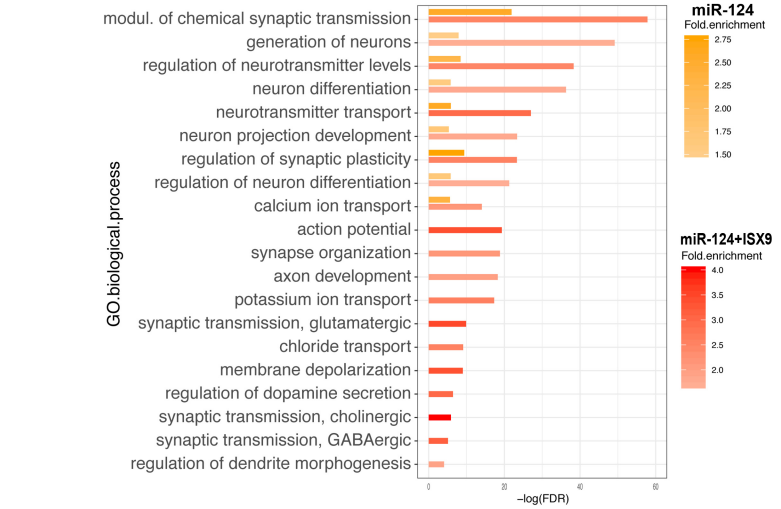
B
GO biological processes for up-regulated genes of miR-124-iNs and miR-124+ISX9-iNs
modul. of chemical synaptic transmission
generation of neurons
regulation of neurotransmitter levels
neuron differentiation
neurotransmitter transport
neuron projection development
regulation of synaptic plasticity
regulation of neuron differentiation
calcium ion transport
action potential
synapse organization
axon development
potassium ion transport
synaptic transmission, glutamatergic
chloride transport
membrane depolarization
regulation of dopamine secretion
synaptic transmission, cholinergic
synaptic transmission, GABAergic
regulation of dendrite morphogenesis
GO.biological.process
−log(FDR)
miR-124
Fold.enrichment
2.75
2.50
2.25
2.00
1.75
1.50
miR-124+ISX9
Fold.enrichment
4.0
3.5
3.0
2.5
2.0

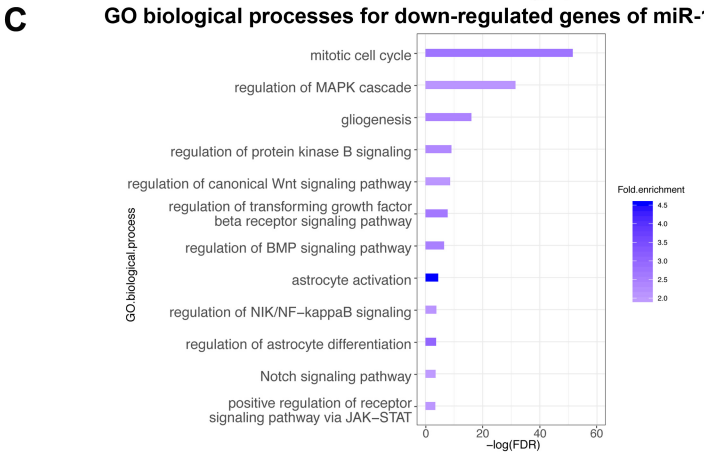
C
GO biological processes for down-regulated genes of miR-124-iNs
mitotic cell cycle
regulation of MAPK cascade
gliogenesis
regulation of protein kinase B signaling
regulation of canonical Wnt signaling pathway
regulation of transforming growth factor beta receptor signaling pathway
regulation of BMP signaling pathway
astrocyte activation
regulation of NIK/NF−kappaB signaling
regulation of astrocyte differentiation
Notch signaling pathway
positive regulation of receptor signaling pathway via JAK−STAT
GO.biological.process
−log(FDR)
Fold.enrichment
4.5
4.0
3.5
3.0
2.5
2.0

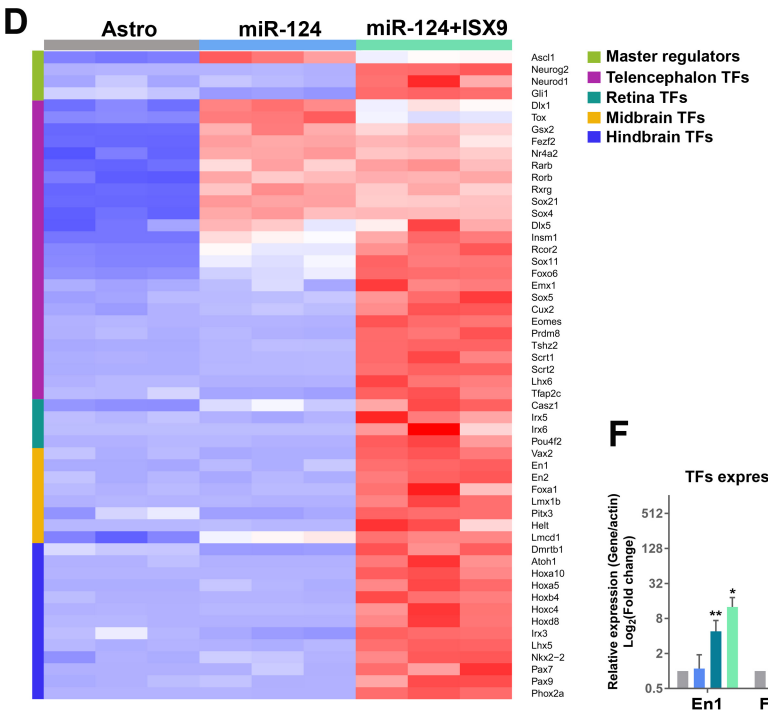
D
Astro
miR-124
miR-124+ISX9
Ascl1
Neurog2
Neurod1
Gli1
Dlx1
Tox
Gsx2
Fezf2
Nr4a2
Rarb
Rorb
Rxrg
Sox21
Sox4
Dlx5
Insm1
Rcor2
Sox11
Foxo6
Emx1
Sox5
Cux2
Eomes
Prdm8
Tshz2
Scrt1
Scrt2
Lhx6
Tfap2c
Casz1
Irx5
Irx6
Pou4f2
Vax2
En1
En2
Foxa1
Lmx1b
Pitx3
Helt
Lmcd1
Dmrtb1
Atoh1
Hoxa10
Hoxa5
Hoxb4
Hoxc4
Hoxd8
Irx3
Lhx5
Nkx2−2
Pax7
Pax9
Phox2a
Master regulators
Telencephalon TFs
Retina TFs
Midbrain TFs
Hindbrain TFs

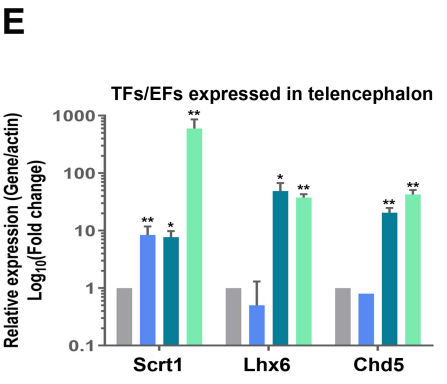
E
TFs/EFs expressed in telencephalon
Relative expression (Gene/actin)
Log10(Fold change)
1000
100
10
1
0.1
Scrt1
Lhx6
Chd5

F
TFs expressed in midbrain
Relative expression (Gene/actin)
Log2(Fold change)
512
128
32
8
2
0.5
En1
Foxa1
Lmx1b

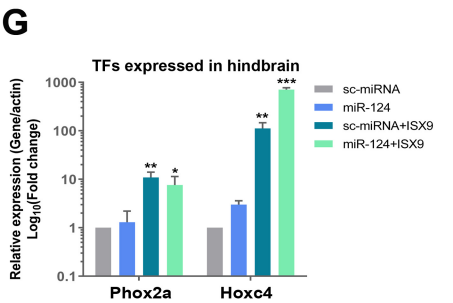
G
TFs expressed in hindbrain
Relative expression (Gene/actin)
Log10(Fold change)
1000
100
10
1
0.1
Phox2a
Hoxc4
sc-miRNA
miR-124
sc-miRNA+ISX9
miR-124+ISX9

Figure 5

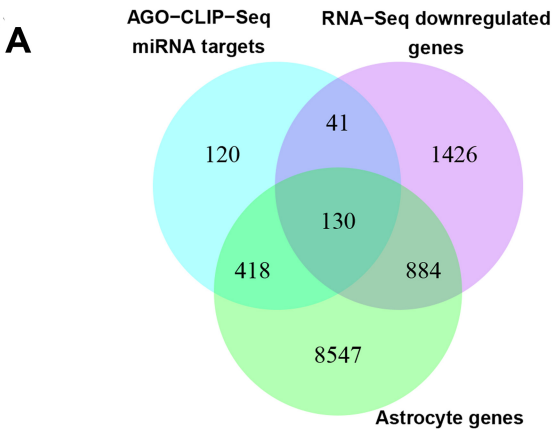
A
AGO−CLIP−Seq miRNA targets
RNA−Seq downregulated genes
120
41
1426
130
418
884
8547
Astrocyte genes


B
Mouse
chr12:80109221-80109245
mmu-miR-124-3p
5′- U A A G G C A C G
3′- G U U C C G U G A
C G G U G A A U G C C- 3′
U U C A A C G A A G A C A U U U- 5′
Zfp36l1
Human
chr14:68789157-68789181
hsa-miR-124-3p
5′- U A A G G C A C G
3′- G U U C C G U G A
C G G U G A A U G C C A A- 3′
U U C A A C G A A G A C A U U U- 5′
ZFP36L1

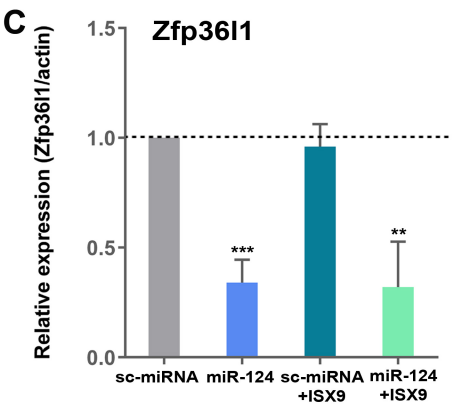
C
Zfp36l1
Relative expression (Zfp36l1/actin)
1.5
1.0
0.5
0.0
***
**
sc-miRNA
miR-124
sc-miRNA +ISX9
miR-124 +ISX9

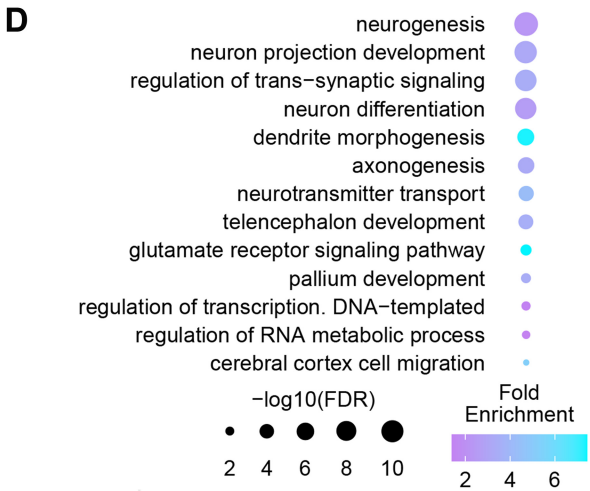
D
neurogenesis
neuron projection development
regulation of trans−synaptic signaling
neuron differentiation
dendrite morphogenesis
axonogenesis
neurotransmitter transport
telencephalon development
glutamate receptor signaling pathway
pallium development
regulation of transcription. DNA−templated
regulation of RNA metabolic process
cerebral cortex cell migration
−log10(FDR)
2 4 6 8 10
Fold Enrichment
2 4 6

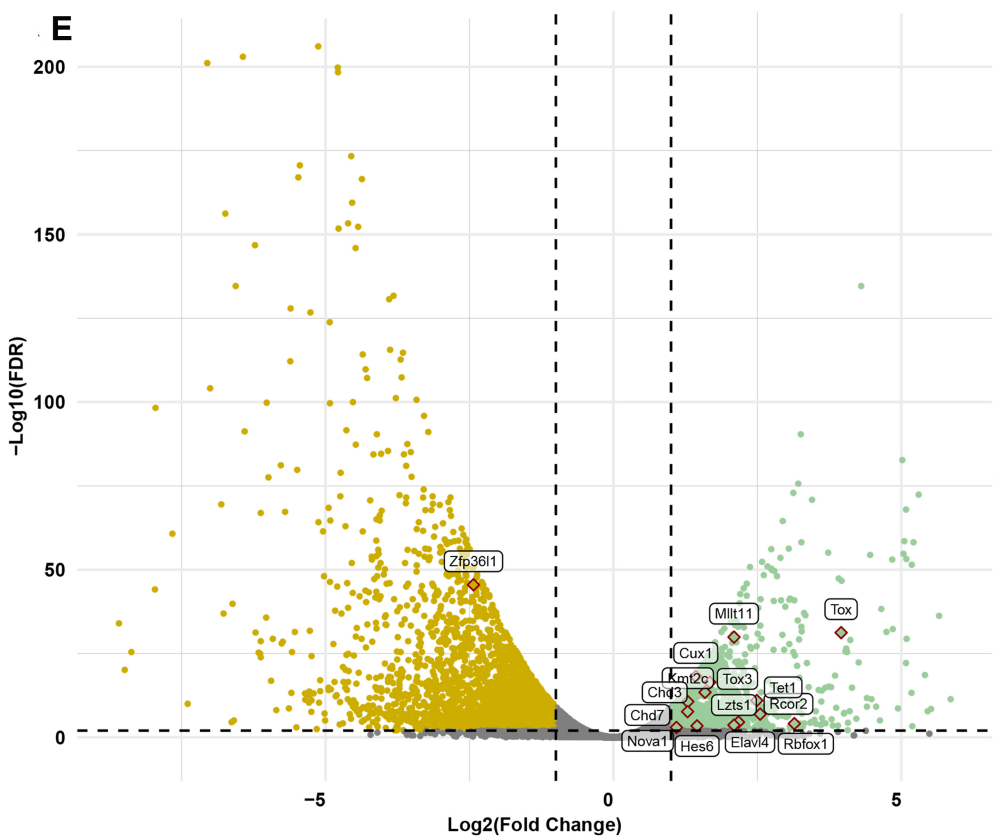
E
200
150
100
50
0
−Log10(FDR)
Zfp36l1
Mllt11
Tox
Cux1
Kmt2c
Tox3
Chd3
Tet1
Lzts1
Rcor2
Chd7
Nova1
Hes6
Elavl4
Rbfox1
−5
0
5
Log2(Fold Change)

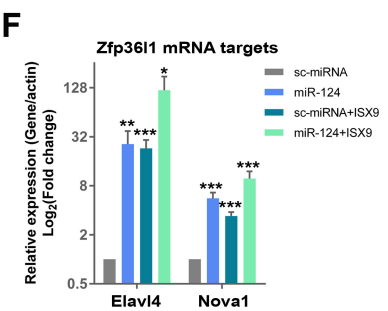
F
Zfp36l1 mRNA targets
sc-miRNA
miR-124
sc-miRNA+ISX9
miR-124+ISX9
Relative expression (Gene/actin)
Log2(Fold change)
128
32
8
2
0.5
Elavl4
Nova1

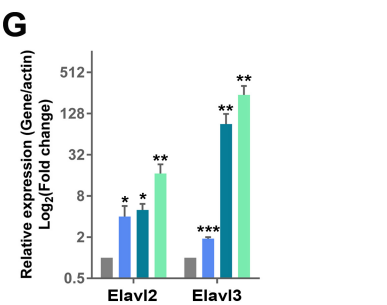
G
Relative expression (Gene/actin)
Log2(Fold change)
512
128
32
8
2
0.5
Elavl2
Elavl3

Figure 6

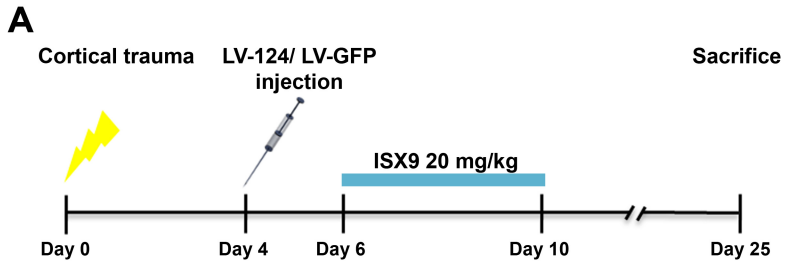
A
Cortical trauma
LV-124/ LV-GFP injection
Sacrifice
ISX9 20 mg/kg
Day 0
Day 4
Day 6
Day 10
Day 25

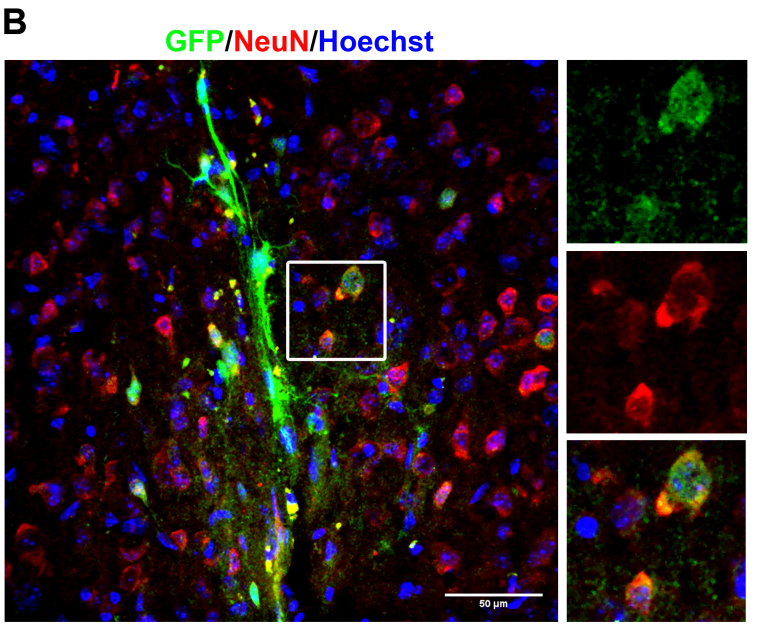
B
GFP/NeuN/Hoechst
50 µm

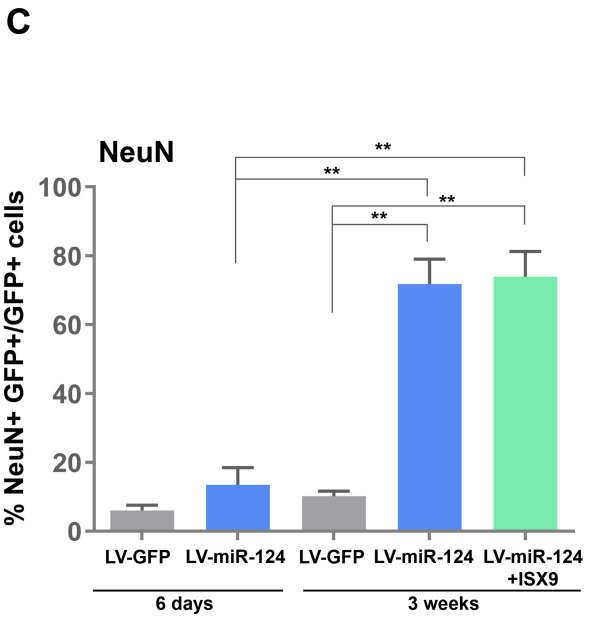
C
NeuN
% NeuN+ GFP+/GFP+ cells
100
80
60
40
20
0
**
**
**
**
LV-GFP
LV-miR-124
LV-GFP
LV-miR-124
LV-miR-124 +ISX9
6 days
3 weeks

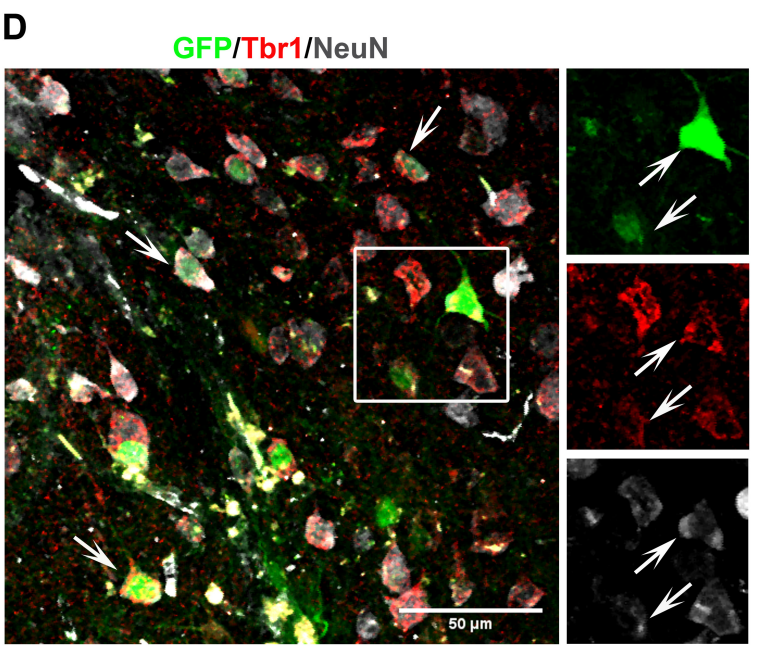
D
GFP/Tbr1/NeuN
50 µm

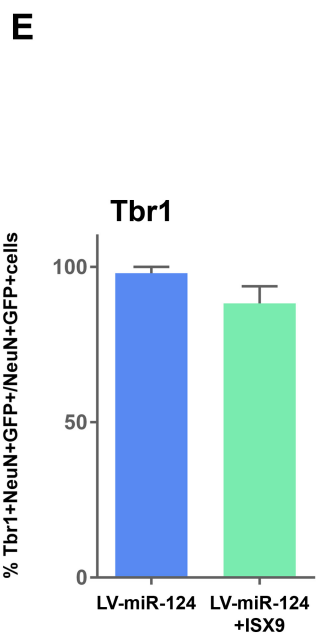
E
Tbr1
% Tbr1+NeuN+GFP+/NeuN+GFP+cells
100
50
0
LV-miR-124
LV-miR-124 +ISX9